NGU Report 93.046

Airborne radon hazard mapping - Løten Hedmark county, Norway

NORGES GEOLOGISKE UNDERSØKELSE

Postboks 3006 - Lade
7002 TRONDHEIM
Tlf. 47 73 90 40 11
Telefax 47 73 92 16 20

REPORT

Report no. 93.046 | ISSN 0800-3416 | Grading: Open

Title:
Airborne radon hazard mapping - Løten, Hedmark County, Norway.

Author:
Peter Walker

Client:
NGU

County:
Hedmark

Commune:
Løten

Map-sheet name (M=1:250.000)
Hamar

Map-sheet no. and name (M=1:50.000)
Løten 1916-I

Deposit name and grid-reference:

Number of pages: 50 Price: Kr. 300,-

Map enclosures: 12

Fieldwork carried out:	Date of report:	Project no.:	Person responsible:
July 1992	Sept 1994	61.2591.01	Jan S. Rønning

Summary:

An airborne geophysical survey with ground follow-up work has been conducted in the Løten area with the intention of mapping the radon gas hazard from the alum shales in the region. The survey was conducted in two phases, with the first phase being the airborne survey. In this phase, the shales were located with combined electromagnetic and radiometric measurements. In the second phase, ground follow-up measurements were used to establish the correlation of the airborne measurements with radon gas in the soil and ground water. Further comparison of the airborne data with radon emanation and concentration data in houses has established that the airborne data can be used to locate areas with significant probability of having high radon gas accumulations.

Keywords: Geofysikk	Radiometri	Radonmåling
		Fagrapport

CONTENTS

ATTACHED MAPS (reduced in scale 1:131.000)

93.046-01	Total Magnetic Field
-02	VLF, orthogonal channel
-03	VLF, inline channel
-04	Apparent resistivity, 4218 Hz
-05	Apparent resistivity, 4616 Hz
-06	Apparent resistivity, 34262 Hz
-07	Potassium, counts pr. sec
-08	Uranium, counts pr. sec
-09	Thorium, counts pr. sec
-10	Potassium/uranium Ratio
-11	Potassium/uranium Ratio
-12	Uranium/thorium Ratio

1 INTRODUCTION

There are various sources of environmental radioactivity which can adversely affect human health if exposure to them is long enough. Some of these are the result of human activity. Others are due to natural sources, and of the natural sources, radon gas is thought to be the most important. Radon is a product of either uranium or thorium decay, and although several isotopes of radon exist, the one with the longest half-life and thus considered to be the greatest concern is ^{222}Rn, a decay product of ^{238}U.

Radon is an inert gas and can thus migrate through the soil and accumulate in dwellings through diffusive, convective and advective processes. Because radon is chemically inert, it is not considered to be a particular hazard to health in and of itself. Rather, the health risk is a result of its short lived decay products, ^{218}Po, ^{214}Pb and ^{214}Bi, all of which are chemically reactive and can thus be adsorbed onto lung tissues.

Radon has been attributed to causing 13,000 to 16,000 lung cancer deaths per year in the United States; links to childhood leukemia are suspected (Nazaroff, 1992). Simple arithmetic based on population ratios would imply a death rate attributable to radon in Norway between 200 and 250 deaths per year. Naturally, such a figure would only be applicable if radon were equally available in both countries. In Norway a major source of radon gas is the uraniferrous alum shales which occur in the vicinity of the Oslo graben. These shales extend in a discontinuous belt which starts in the Oslo fjord area and extends northwards to the Hamar / Løten region through a relatively densely populated part of the country.

The distribution of hazard from radon is far from uniform, and depends largely on the local properties of soils and bedrock, as well as upon building construction techniques. In the Løten area, for example, Statensstrålevern, has measured the concentration and exhalation rates since at least 1986. Data provided to NGU by Statensstrålevern indicates that several dwellings are over the Norwegian guideline recommmended for taking remedial action, of approximately 200 Bq/m^3 (Statens Inst. for Strålehygiene, 1991). In fact, one dwelling visited by myself in the course of our work in Løten had, according to a letter from Statensstrålevern, concentrations of radon gas of 80 times this remediation threshold. Given the high direct and indirect costs of cancer treatment, it is clearly in the public interest to map the distribution of radon and thus the spatial distribution of the associated health hazard. If the presence of radon could be successfully mapped, preventative measures could then be taken both to reduce the associated health hazard in highly affected areas, as well as providing guidance when erecting new structures.

In this report, the use of airborne geophysical measurements for mapping radon gas in soils is evaluated, and is an extension of work carried out in the United States by a number of

workers. Previous work comparing soil gas radon with airborne and ground radiometric measurements has been published by Duval (1990), who reported on work in Colorado, USA. Duval concluded that, with caveats, surface gamma ray data can be used to estimate amounts of radon gas in soils.

The presence of elevated radon gas in the ground has also, in one study at least, been correlated with elevated radon gas readings in dwellings. Harrell et. al (1991, Figure 6) reports that increases in radon concentrations in the Ohio Shale correlate with increases in median basement radon concentrations in dwellings. Taken a further step, work cited in a review by Neilson et. al (1991) indicated that airborne radiometric measurements in New Jersey could be used to outline areas with elevated radon concentrations inside dwellings.

Similar application of airborne geophysical measurements can doubtlessly be applied to mapping radon associated with the the alum shales in southern Norway. To investigate this possibility, NGU flew a combined radiometric and electromagnetic helicopter survey in the Løten area during the summer of 1992 (see Figure 1). The radiometric component of the survey mapped the surficial distribution of uranium source directly, whist the electromagnetic component of the survey was used to map the shale source rocks. Followup verification with ground measurements of the soil gas component of radon, and comparisons with radon emanation and concentration data taken from dwellings show the viability of the airborne radiometric method for mapping the distribution of radon, and thus the associated health hazard, in the Løten area. Further followup investigations of radon in ground water demonstrates that the presence of shale affects the concentration of ground water radon.

Aside from the airborne geophysical maps produced during the course of this work, one result of this work then, is a model with some capability for predicting the presence of radon gas in dwellings in the Løten area. Although the model is far from complete, it can be used to convert airborne geophysical measurements into a measure of the probability that radon will enter dwellings in the Løten area from either the ground or the ground water supply. Results of this study form a basis for further research for improving the model for predicting the presence radon gas from airborne geophysical measurements, and justification for extending the airborne survey into adjacent areas.

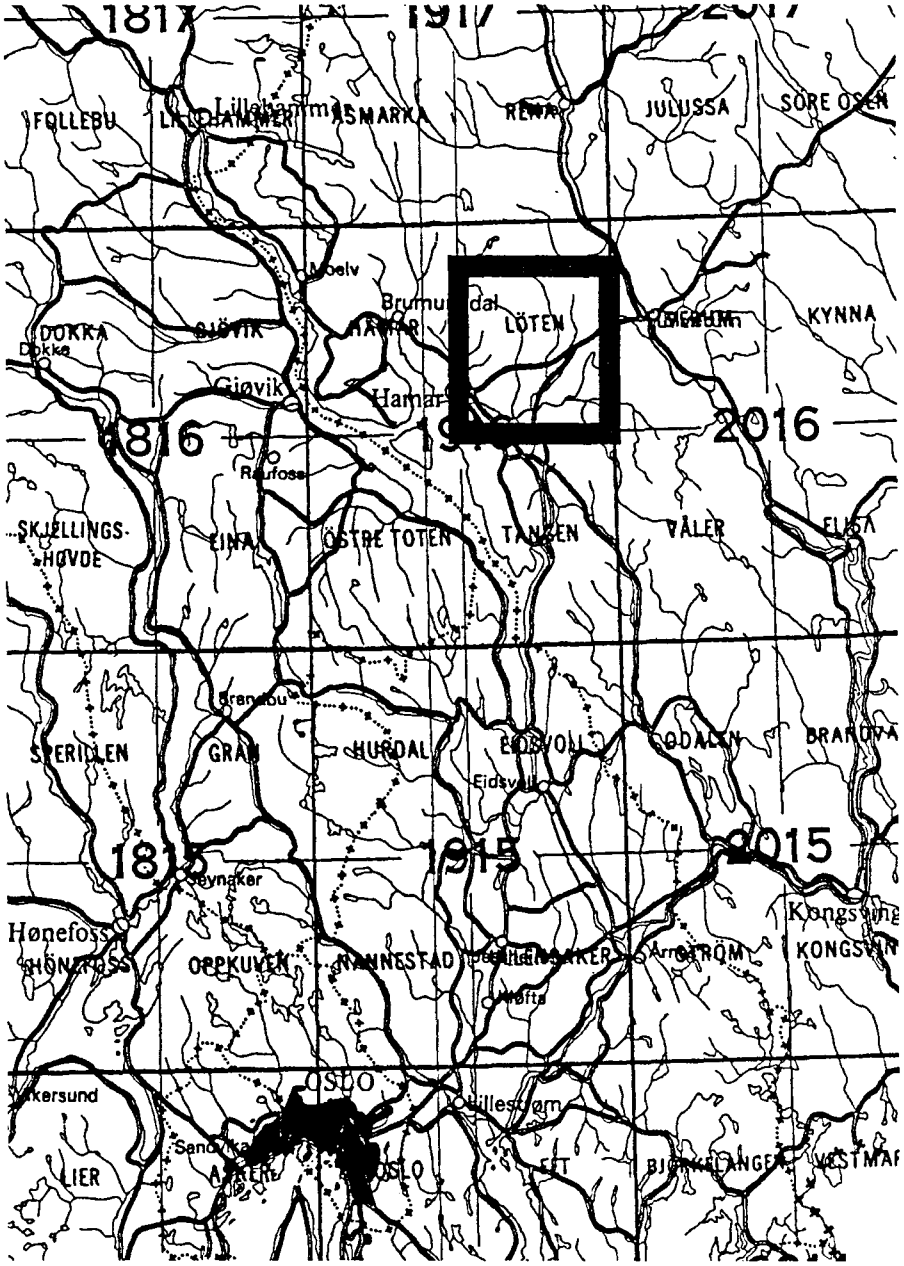

Figure 1. Surveyed area southern part of map sheet 1916 I Løten

2 BACKGROUND DATA

2.1 Alum Shales

The alum shales in the Løten area were formed in a shelf environment from the middle Cambrian to the early Ordovician. They occur stratigraphically over lower Cambrian sandstones which grade into siltstones and are overlain by limestones and shales formed in the middle Ordovician. The shales in Løten are not unique in Scandinavia. Rather, the unit is thought to extend through Sweden and into the Gulf of Bothnia, south into Denmark (Gee, 1980). The Løten shales then, are thought to form part of a larger unit deposited in a shelf environment on the Baltoscandian platform

According to Andersson et al (1985), the shales formed the detachment zone for the stratigraphically lowest nappes associated with the Caledonian front, and in places have been highly strained by thrusting. In southern Norway, the alum shales outcrop along a belt which extends from Langesundfjord and Oslofjord in the south, northward along the Oslo graben to the Hamar and Løten areas. According to Skjeseth (1958), the shale occurrances in the southern part of the graben tend to be relatively undisturbed by the Caledonian orogeny. Faulting and folding increase towards the north. Where the shales lie close to the Permian intrusives of the Oslo Graben, they can be locally altered to hornfels. Figure 2 illustrates the occurrances of alum shales in southern Norway, reproduced from Skjeseth (1958).

The alum shales are distriguished by a geochemical signature which includes a high content of organic carbon, uranium and vanadium, with the uranium being distictively concentrated in the Upper Cambrian strata. The shales are named for their alum salt, a hydrated potassium aluminum sulphate, and were exploited for this in Sweden three hundred years ago. In Norway, the alum shales have an organic carbon content, averaging 10% in the Oslo Graben (Bjørlykke, 1974), with carbon contents of between 40 and 50% reported by Foslie (1919) in the Gjøvik area. Sulphur is also characteristic of the alum shlaes, and Bjørlykke (1974) reported that they contained sulpher contents of upto 12%.

In the Oslo graben, several zones have been identified which have uranium content averaging up to 150 ppm over several meters (Skjeseth, 1958) , and vanadium content has been measured at 2000 ppm in places. Within the shales, the occurrance of uranium tends to be highest where the organic carbon content is largest, but the relationship between the two is by no means linear or pervasive. In the Elsjø area for example, Olerud (1984) for example reports poor linear correlation coefficients between carbon and uranium of 0.25 and -0.07. This low correlation probably reflects a redistribution of uranium mineralization from local hydrothermal activity associated with Permian intrusives.

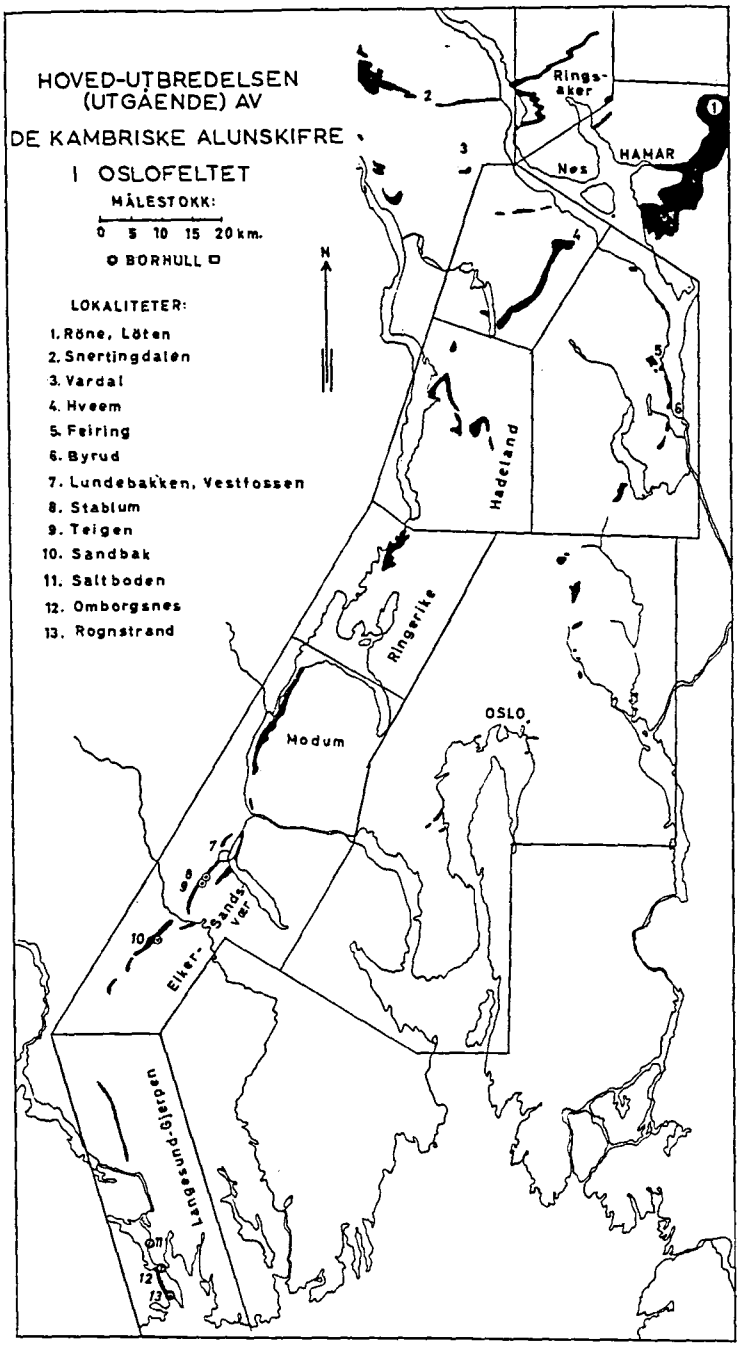

Fig. 1. Kambrisk alunskifer i Oslofeltet og tilgrensende områder.

The main distribution of the Cambrian Alum shales in the Oslo Region and adjacent districts.

Figure 2. Alum shales in the Oslo region (reproduced from Skjeseth, 1958).

2.2 Previous Mapping in the Løten Area

The bedrock geology of the Løten area has been mapped at 1:50,000 scale by Bjørlykke et. al, 1980 (Figure 3). The eastern four kilometers of the sheet are characterized Precambrian igneous rocks, which are overthrust by lower Palaeozoic sediments from the northwest. To the north of the map sheet area, the surficial geology is dominated by Precambrian sandstones and quartiztes have been overthrust onto the lower paleozoic sediments. Rifting during the Permian has resulted in a series of north-south trending faults with downward movement on the east side which subsequently cut the overthrust sediments and basement rocks alike. Movement along these faults displaced rocks on the west side of the faults upwards in relation to those on the east.

The lower Palaeozoic sediments have been mapped as three groups, the Bjørge Formation on the top which consists of middle Ordovician didymograptus and ogygiocaris shales, the Stein Formation consisting of lower Ordovician Orthoceras limestones which have been partly folded with Cambro-Ordovician shales and an undifferentiated seres of Cambrian and lower Ordovician sandstones, shales and alum shales. The alum shales which are located in the latter undifferentiated series are of principal interest in this report, and have not been mapped as separate a distinct unit.

The quaternary geology of the Løten area has been mapped by Follestad (1973), and is dominated by moriane material with minor occurrances of bog and glacial fluvial deposits. Ice motion is interpreted to be from the north. According to Skjeseth (1958), glaciation heavily eroded the alum schists in the Løten. As a consequence there are areas where eroded alum shales comprise a significant fraction of the overburden, as for example occurs at the Røne farm. From the ground followup work done during this project, it was apparent that this fraction was often large enough to colour the earth black, and that this black earth had radon levels which were elevated significantly over backgrounds in the Hamar area. This may indicate that significant amount of the radon detected during this investigation is due to glacially transported schists in the overburden, rather than due to the bedrock schists themselves.

Ground water pH levels of between 6 and 7 generally correlate well with the Cambro-Ordovician deposits. More acid waters are associated with the granitic rocks to the east.

A fixed wing airborne electromagnetic and radiometric survey was flown over the area in 1967 (NGU 1967a og b). Results of that survey are illustrated in figures 4 and 5 on the following pages.

Figure 3. *Bedrock map 1916 I LØTEN.*

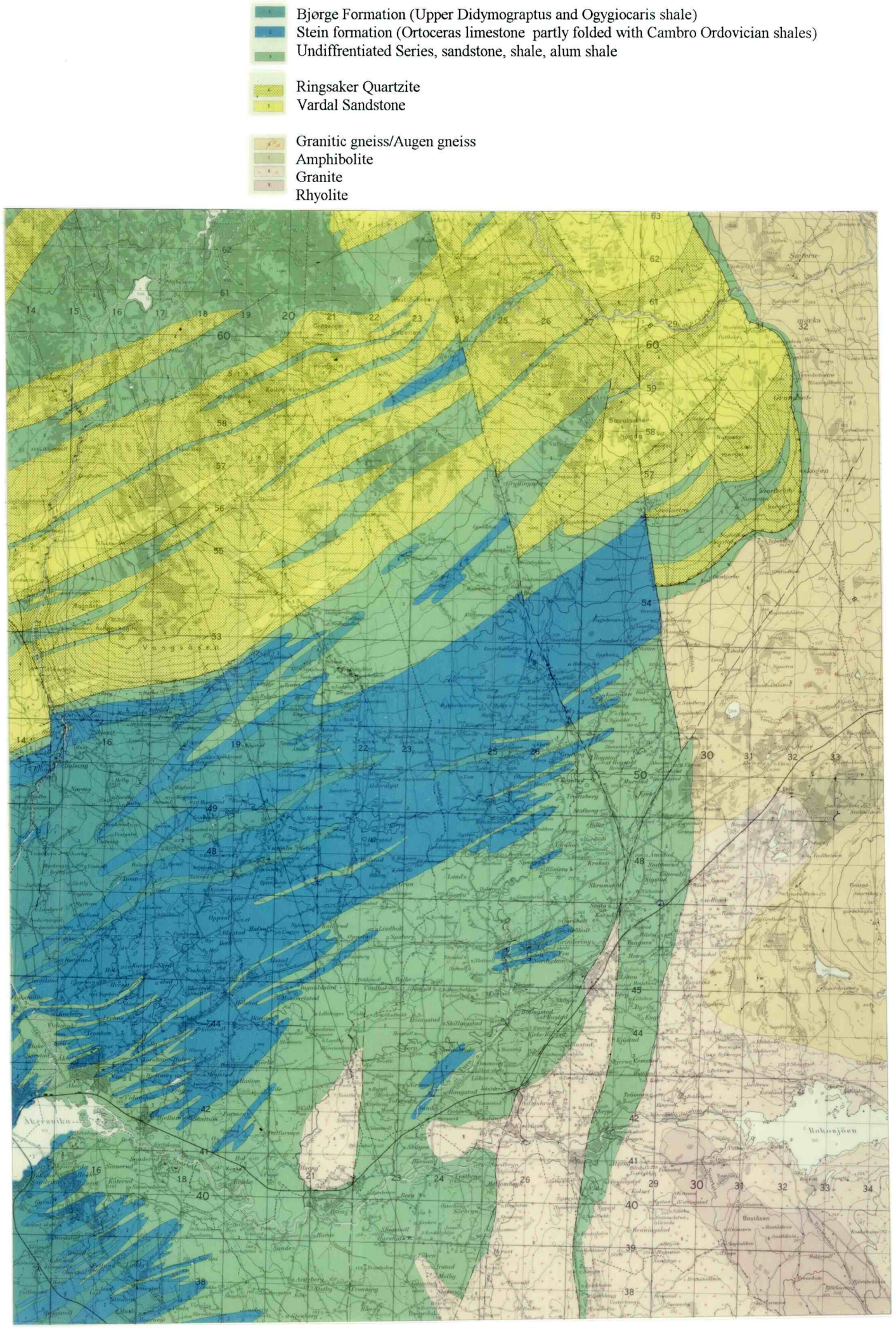

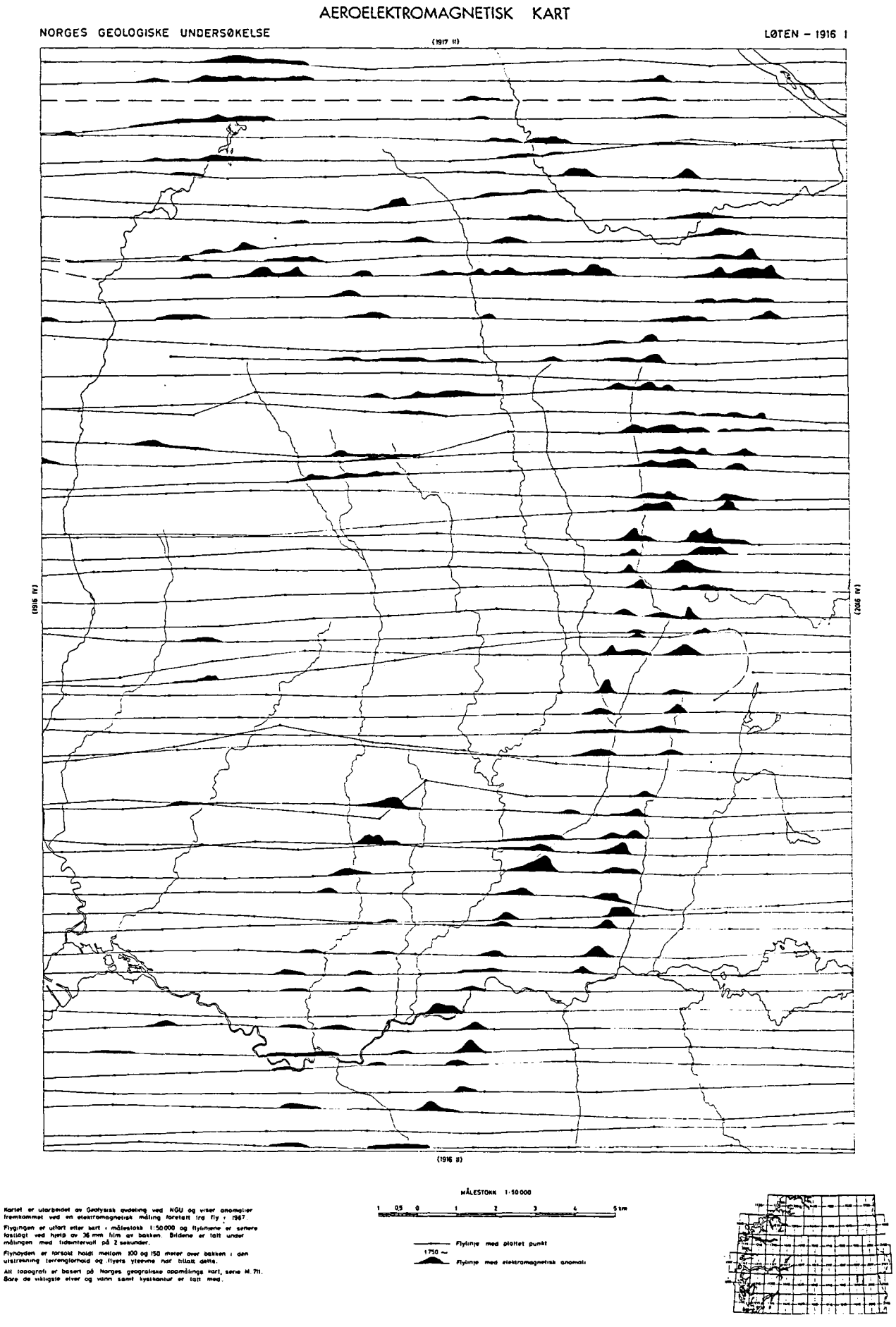

Figure 4. Airborne electromagnetic survey results, 1967

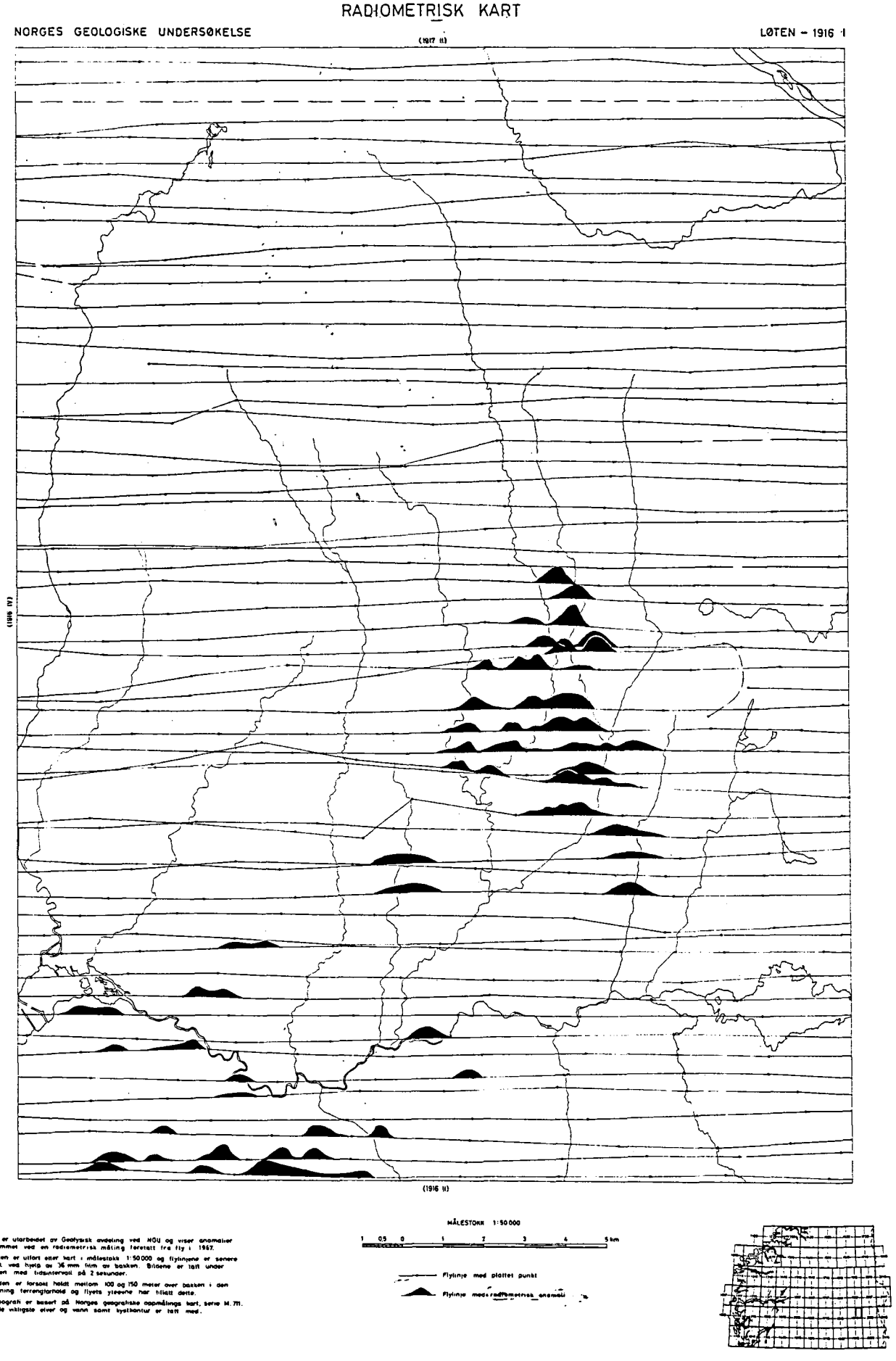

Figure 5. Airborne radiometric survey results, 1967

3 BACKGROUND TO A PREDICTIVE MODEL

A major objective behind the work undertaken in this report is to determine if and how airborne geophysical measurements can contribute to our understanding of the location of radon gas in Norway. In order to do this, it is first necessary to understand the behavior of radon gas in the ground, and how radon might thus be measured. Once this is understood, a relationship between the airborne measurements and the presence of radon gas in soils and then dwellings can then be developed.

3.1 The ^{238}U Decay Chain and Remote Radon Measurement

Three varieties of radon exist, ^{219}Rn which is generated as a consequence of the decay of ^{235}U, ^{220}Rn from ^{232}Th and ^{222}Rn from ^{238}U. Of these, the isotope of primary concern is ^{222}Rn, as this is the longest lived isotope of the three with a 4 day half-life. With half-lives of 51 and 4 seconds respectively, ^{220}Rn and ^{219}Rn tend to decay before migrating through the ground any significant distance, and thus tend not to be considered so hazardous.

The ^{238}U decay chain is illustrated schematically in figure 6, which is derived from Nararoff (1992) and Rose et al (1979). The ^{238}U parent has a half-life of approximately four billion years, and decays through a series of intermediate steps to ^{226}Ra with a half-life of approximately 1600 years. Radium thence decays to ^{222}Rn, with a half life of approximately 4 days, and then through a series of short lived daughter products namely , ^{218}Po, ^{214}Pb, ^{214}Bi and eventually to ^{206}Pb through ^{210}Pb. It is the chemically reactive daughter products of radon, namely ^{218}Po, ^{214}Pb and ^{214}Bi which are considered present the health hazard associated with the presence of radon gas (Nazaroff, 1992).

It is this natural decay of uranium which is exploited in airborne radiomentric measurements. Uranium can be detected with a gamma ray spectrometer which is used to count the disintegration rate of a particular member of the uranium decay series. In most cases, the uranium decay itself is not detected, but instead the decay of ^{214}Bi is used. Since the nuclear decay rate of an isotope is directly proportional to the number of that isotope present, the decay rate of ^{214}Bi is directly proportional to the amount of ^{214}Bi isotope available. If all the isotopes in the decay series are be assumed to be in equilibrium, then uranium concentration can be calculated directly from the concentration of ^{214}Bi. Frequently however, geochemical processes act which separate the daughter products from the parent isotopes, and radiogenic equilibrium is not present. Thus although it is possible from gamma ray measurements to compute a concentration of uranium from the count rate, this concentration is generally referred to as an effective concentration in observance of the fact that all elements in the decay series may not be in equilibrium.

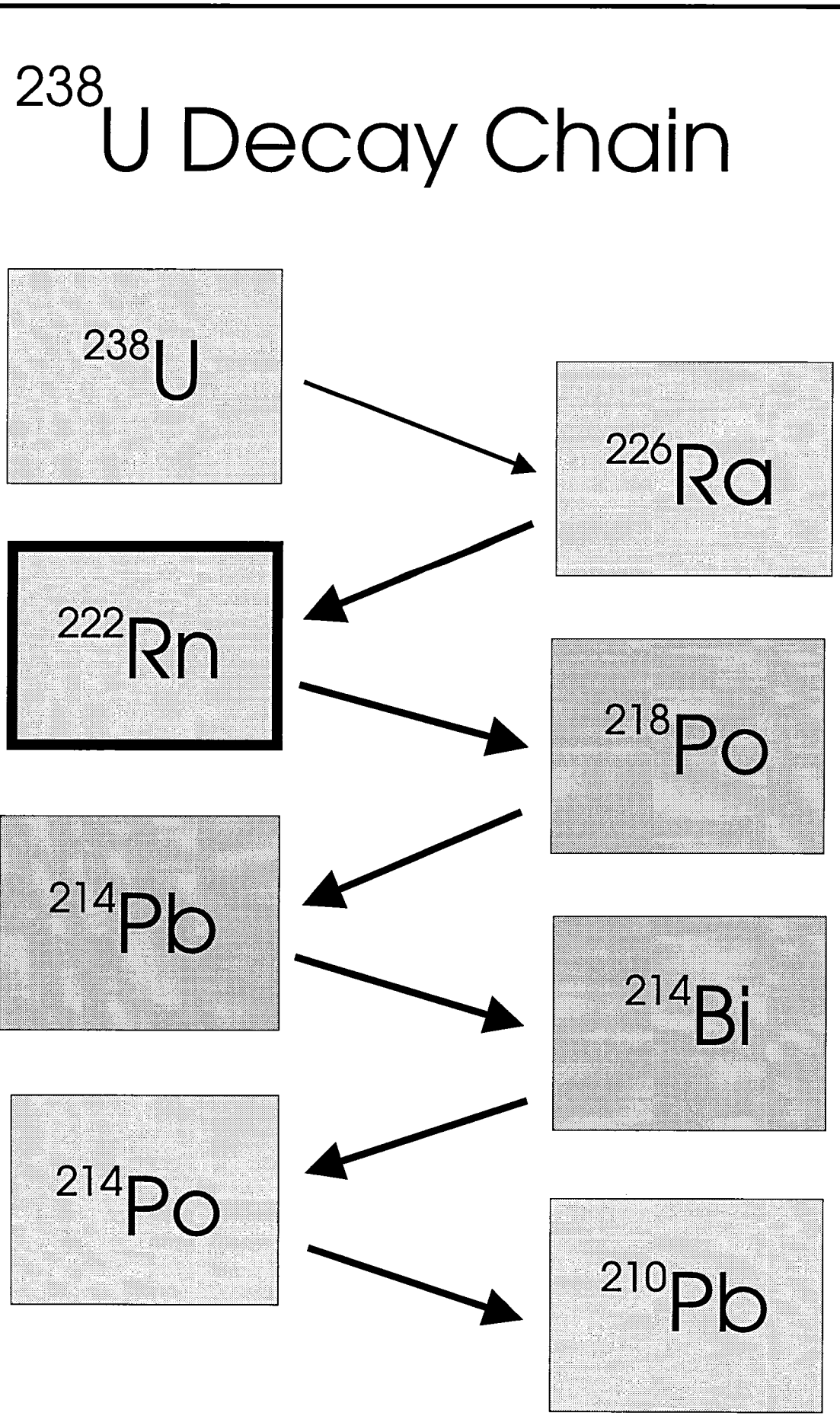

Figure 6. ^{238}U *decay chain*

Since radon is also a parent of ^{214}Bi, the presence of radon can also be inferred from the presence of ^{214}Bi. In this case however, using the decay of ^{214}Bi to infer the concentration of radon is somewhat more reliable than using it to infer the concentration of uranium since the intervening isotopes are short lived. ^{214}Bi is thus more likely to be in radiogenic equilibrium with the parent radon isotope than with the parent uranium isotope.

3.2 Uranium, Radium and Radon Geochemistry

Uranium is mobile in oxidizing environments, particularly when acid or carbonate rich, but fairly immobile in reducing environments (Rose, 1979). Units such as the alum shales which are rich in organic carbon would be expected to be reducing, and Harrell et. al (1991, Figure 3) have found a positive correlation between the uranium concentration and the total organic carbon in the Ohio shale. Studies previously cited on the alum shales in the Oslo graben have indicated similar behaviour. Organic carbon seems to promote the retention of uranium present in the shale.

The immobility of uranium in reducing environments does not necessarily apply to its daughter products. Radium, for example, (Gregg and Holmes, 1991; Rose et. al, 1979) is fairly mobile in reducing environments in relation to uranium, but is immobile in oxidizing environments. Thus radon may emanate from sources which may be significantly displaced from the uranium host rock if the intervening radium decay product has been mobilized in the reducing environment and has then later immobilized by contact with a more oxidizing environment.

Radon itself is an inert noble gas, and so is not subject to the same geochemical processes as uranium and radium are. It is nevertheless, very soluable in water, and this soluability can enhance its mobility where ground water is in contact with radon source minerals. Its mobility, however, is limited by its halflife.

The high carbon content of the alum shales undoubtably generates a locally reducing environment, and the uranium found in the carboniferrous alum shales bedrock is expected to be fairly immobile. Greater mobility is expected where the shales are in contact with carbonate rich water such as might be derived from the limestones in the Stein Formation. In areas where the shales have been dispersed in overburden due to glacial erosion, one may expect the uranium to be more mobile than it would be in the bedrock alum shales.

Since organic carbon is frequently a good conductor in sedimentary and metamorphic rocks, this association of uranium with organic carbon suggests that the airborne electromagentic

technique could be applied to delineating shales which are likely to contain a high probability of containing uranium.

3.3 The Generation of Free Radon Soil Gas

Radon is generated through nuclear decay, often at sites in crystal lattices which are located inside soil grains. For the derivative radon to escape to the surface it must first enter the pore spaces in the soil and then migrate to the surface. The fraction of gas that actually enters the pore space is termed the emanation power of the soil.

Radon atoms are thought to enter the pore space with the recoil energy they acquire through the nuclear decay. If a radon atom is to be released into the environment, the atom must be given sufficient energy to reach a pore space. Factors affecting the amount of gas actually reaching the pore space include the competency of the intervening lattice and the average size of the soil grains. The probability that a particular atom will actually be trapped in a pore space depends on the porosity of the soil. This probability is enhanced by the presence of water in the pore space which serves to dissipate the recoil momentum before the atom penetrates and is trapped in adjacent grains. Water plays a dual role: while it increases the emanation power of the soil, it also reduces the permeability of the soil to gas flow.

Free radon is also generated by the radioactive decay of radium which has been dissolved in the pore water itself. Because radium tends to be mobile in reducing environments where uranium is bound, it is possible for the radium, and hence the radon so created, to be significantly displaced from the parent uranium mineralization.

3.4 The Migration of Radon Through Soils

Because radon is short lived, for it to migrate any significant distance it must have both an available pathway and an effective transport mechanism. Pathways are believed to be fractures, and capilliaries in soils ranging from 0.001 cm to .025 cm in diameter (Cui, 1990). As a result, clays and water saturated soils where the capillaries are saturated with water tend to be relatively impervious to radon migration.

Mechanisms for radon transport through soils are complex, and consist of components attributed to diffusion, convection and advection. Of the three, advection is considered to be the mode which results in the eventual entry of radon gas into buildings. According to Harrell

et. al (1991), little if any radon would survive diffusion through the ground past a distance of approximately 6 meters even under optimum soil moisture and porosity conditions. Advection on the other hand, could draw radon from considerably deeper depths as a result of low pressure conditions on the surface created by weather systems, low pressures due to strong winds or from the downward percolation of rain water. Under such conditions, Harrell believes that significant amounts of radon could rise from depths of 15 meters under ideal soil transport conditions, or deeper in the presence of fractures. Nazaroff (1992) however quotes studies which indicate that diffusion dominates advection where radon gas enters the atmosphere from soils, but that advective processes tend to dominate diffusive ones where radon enters buildings. Others (Gregg and Holmes 1991) consider that convective processes using a carrier such as soil gas or ground water to be the dominant transport mechanism. There seems to be little consensus in the literature then, as to which of several processes dominates the flow of radon through soils.

3.5 Radon Entry and Accumulation in Buildings

According to Nazaroff (1992), advective transport dominates diffusive transport of radon into buildings. There are two reasons for this; firstly building foundations usually pose a barrier to gas diffusion, and secondly building heating and ventilating systems, as well as the flow of wind around the building itself, cause a pressure reduction in buildings relative to the outside air, thus promoting the entry of gasses from the adjacent soils. Typical places where gas could enter would be through cracks in foundation walls and basement floors, floor drains or other buried service accesses.

Winds promote advective entry of soil gas into buildings by lowering the pressure inside buildings as they are deflected around them. When the building is in contact with the underlying soil, this wind action sets up a pressure gradient between the bottom of the building and the soil underneath. This pressure differential tends to draw soil gas into buildings, particularly in buildings which have excavated basements.

Advective entry is also promoted by heating systems. In heated buildings, a vertical pressure differential is set up with the outside air which tends to draw air inward at the base of the building and outward at the top of the building. Thus, particularly in winter months, when buildings are both heated and are closed more tightly to the outside air, the operation of heating systems will tend to promote soil gas entry and accumulation inside buildings.

In addition to advective transport, radon may also enter buildings dissolved in well water supply. Release of radon gas into the building would occur in this case as water is used,

with release rate being particularly high when the water is highly agitated such as would occur from washing.

Radon entry into buildings, therefore, depends on a number of factors including weather conditions, the water supply and on building construction and operation which cannot be measured by airborne geophysics. Nevertheless, since radon can only enter buildings if it is available to do so, that there is dependency of radon concentration in buildings on the radon gas content in the underlying soils and water supply cannot be in doubt.

3.6 Towards a Predictive Model of Radon Occurrance in Løten

Airborne geophysics should be able to contribute to mapping the distribution of radon in southern Norway. Direct gamma ray measurements should be sensitive to the distribution of radon gas in the ground, although such measurements will not be able to distinguish between the partitioning of bound and mobile radon in soils. Electromagnetic measurements should map the conductive strata containing the organic carbon. Since the organic carbon rich stratum also hosts uranium, electromagnetic data should provide information on the location of radon sources at depth, and thus provide some indication of radon in the ground water supply. Since radium is more soluable than uranium in the alum shales, one may also expect radon in ground water to be dispersed from the conductive zones themselves. Relationships between conductivity and uranium content would be expected to hold in Løten since the shales have not been altered hydrothermally.

Previous work supports the view that airborne measurments can contribute to the understanding of radon hazard. Work cited in a review by Neilson et. al (1991) indicated that airborne radiometric measurements in New Jersey could be used to outline areas with elevated indoor radon concentrations. It was found that radiometric anomalies of greater than 6 ppm effective uranium outlined houses where radon concentration exceeded the US Enviromental Protection Agency remediation threshold. Other workers, for example Duval (1990) and Harrell et. al (1991), have published correlation between radon and uranium.

Although much of this published work relates the occurrance of radon to alum shales, from the work of Harrell (1991) one must also be alert to possibility that uranium can be redistributed into limestones, and that limestone may also therefore serve as a source of radon gas. The Cambrain-Ordovician stratigraphy of the Løten area, as well as glaciation during the quaternary are favourable to such a situation.

4 THE AIRBORNE SURVEY

The helicopter survey was executed during July, 1992, covering an area of 18 approximately 500 square kilometers. Line spacing was nominally 200 meters at a flight elevation of 60 meters, with infill lines flown over the radiometrically interesting part of the survey area at a 100 meter separation.

4.1 General description

Survey area: The area was located in Norwegian mapsheet number 1916 I (Løten), and extended east and north from the city of Hamar. The survey area was bounded approximately by UTM coordinates 6737000 N in the south, 6755000 N in the north, 633000 E to the west and 615000 E to the east in UTM zone 32 on the ED-50 ellipsoid. A total of 148 lines were flown.

Equipment: Equipment operated in the survey included a four-frequency electromagnetic system, a optical pumped magnetometer, a VLF-EM system, a γ-ray spectrometer, a video camera for flightline tracking, a radar altimeter and a GPS navigation system with base station for differential corrections. All data were recorded both in digital and in analogue form, with positioning data stored on video film as well as being recorded by the navigator in flight.

Aircraft: The survey was flown using an Aerospatiale Ecureuil B-2 provided by Helikoptertjeneste A/S, based in Kinsarvik, Norway. Geophysical and ancilliary equipment were installed at the Løten airport, which was also used as a base of operations.

Electromagnetic system: Electromagnetic measurements were made using a four-frequency electromagnetic system manufactured by Aerodat, Ltd. of Mississauga, Canada. The system employs two coil pairs which operate at 915 and 4616 Hertz in the coaxial mode, and two pairs which operate at 4218 and 34262 Hertz in the coplanar mode. Transmitter and receiver coils for each frequency are separated by approximately 6.4 meters, and are mounted inside a kevlar "bird" with a total length of approximately 8 meters. The system measures the inphase and quadrature responses at each frequency 10 times per second, which corresponds to approximately a 3 meter interval over the ground at a flight speed of 100 kilometers/hour. The bird is suspended approximately 30 meters below the helicopter. Output of the system is in parts per million of the primary field at the receiver coils.

VLF-EM system: VLF-EM measurements were made with a Herz Totem-2A VLF system. The system measures the field strength radiated from transmitters in the 15 to 30 KHz range

which are operated by various national governments. The system provides total field and vertical quadrature measurements of the fields from two such stations. The sensor was towed in a bird located approximately 10 meters below the helicopter. Station NAA was used as the inline channel whilst GBR was used for the orthogonal channel.

The transmitters used for the VLF component of the survey are:

Abbreviation	*Location*	*Frequency*
GBR	Rugby, England	16.0 KHz.
NAA	Cutler, Maine	24.0 KHz.

Magnetometer: Magnetic measurements were made with a Scintrex split beam optically pumped magnetometer coupled to a digital signal processor. Magnetic data are recorded 10 times per second and the sensor is located approximately 15 meters below the helicopter.

Magnetic base station: Diurnal variations in the magnetic field were recorded with a Scintrex MP-3 magnetometer located at the base of helicopter operations. Data were recorded digitally on a personal computer and in analogue form on a thermal chart recorder. Clocks in the base station and the data acquisition system were synchronized prior to each flight to ensure diurnal effects could be accurately removed from the magnetic profile data.

Radiometrics: Radiometric measurements were recorded with a 1024 cubic inch crystal volume detector which was coupled to a Geometrics gamma-ray spectrometer system. The system consists of 4 crystals which are continuously stabilized by a micro-processor controlled spectrum stabilization package.

Data Acquisition system: Data were acquired by a DAS-8 data acquisition system manufactured by RMS Instruments Ltd. Data were recorded both digitally on a 40 Mbyte tape and in real time with a thermal graphic printer. Digital data were subsequently transferred to a Digital Equipment Corp. VAX at NGU for processing and map production.

Flight path video: As a backup to the GPS navigation system, a video camera was mounted below the helicopter beside the spectrometer. Time and manual fiducials are superimposed on ground imagery to assist the correlation of the video with digitally recorded data.

Radar altimeter: A King KRA-10A radar altimeter was mounted in the helicopter to provide ground clearance information to an accuracy of 5%. The primary use of the radar altimeter as an aid for maintaining constant ground clearance.

4.2 Operational aspects

The survey consisted of 11 flights, the first 7 at a line spacing of 200 meters with the remainder of the flights used for the fill in lines. Weather was sunny for the first part of the survey, later becoming overcast with intermittent rain. Details of various operations are listed below.

Flight path: The survey was flown with a combination of GPS without differential corrections. The quality of the GPS was quite poor during the survey, with jumps of 50 meters quite common. Flight path was reconstructed from the GPS, but is far below the quality typical of helicopter surveys due to the poor performance of the GPS system and the lack of supplemental electronic navigation.

Aircraft ground speed was approximately 60 knots (100 kph) or about 30 meters/second. Aircraft location was controlled in flight horizontally by GPS output and the intrepid author, as navigator, with 1:10000 scale topographic maps. Vertical in flight control was provided by a radar altimeter.

Magnetic basestation: A magnetic basestation was operated so diurnal changes in the magnetic field could be removed from magnetic profile data. The base station was located at Løten airport in a wooded area. The diurnal field was sampled every 4 seconds and was recorded both digitally for later data processing and in analog format to assist in quality control.

EM background lines: Background lines, to monitor instrumental drift in the electromagnetic system, were flown at 20 minute intervals. To reduce instrumental drift, the electromagnetic system was left on continuously so the electronic components would remain warm and so have stable electronic properties.

Spectrometer background lines: . Background lines were flown before and after every flight over Mjøsa for a duration of approximately two minutes.

4.3 Processing

Processing system: Data were processed on a microVAX 3100 using processing software acquired from Aerodat Ltd. Colour maps were produced on a Calcomp 58000 plotter at NGU.

Processing philosophy: Processed products were generated using minimal filtering, interpolation, blending of data between lines while gridding, and with minimal pruning of the data. Grids were filtered only to reduce the raggedness of the contoured product, and not to blend data between lines. Any manual intervention in the levelling of the data is explained in the sections below. Thus the maps produced reflect the quality of the data used to generate them, and not that of an idealized geophysical dataset. For example, there are occasional 50 meter offsets in the flight path which could have been removed by filtering. The resulting flight path, for example, may look worse than if it were filtered, but the result is actually more representative of the quality of the data used to generate it.

Gridding: Contour and colour presentations were prepared from gridded profile data at a 25 meter grid cell spacing. Profile data were gridded by interpolating in a north-south direction. A final grid was then prepared from the two grids, averaging common values where there was overlap between the two separate grids.

Total field magnetics: Diurnal profiles were first plotted and edited to remove spikes. The diurnal variation was then subtracted from the profile data, assuming a base field of 50000 nT. The data were then processed using a spike rejection algorithm and then filtered with a 5 point (0.5 second) Hanning filter. Data were then gridded at 25 meters and contoured, with a 5 by 5 point Hanning filter applied to the grid before contouring.

Following this, a 6 nT heading correction was applied to the profile data to correct for herringboning in the magnetic contours. The data were then regridded and contoured to yield the final contoured product.

VLF: VLF in-line and orthogonal total field channels were processed using a spike rejection algorithm, and then Hanning filtered using a 9 point (1.8 sec) filter. The VLF data were then contoured and manually pruned to eliminated anomalies along line which could obviously have no geological origin. The data were re-gridded and filtered with a 5 by 5 point Hanning filter before contouring.

EM: Electromagnetic profile data were despiked, Hanning filtered and then converted into calibrated ppm values using constants supplied with the EM system. Background lines (those flown at 1000 feet or more to measure electronic system drift) were more heavily filtered than profile lines, to establish a better zero level, and of course because there was no point in minimizing the filtering to assure good spatial resolution of EM anomalies there.

EM data were then baselined to remove electronic drift. From these data, apparent resistivities were computed at each frequency. The apparent resistivity was then gridded, filtered with a 5 by 5 point Hanning filter and then contoured.

Radiometric data: The radiometric data were processed using software originally developed by Geometrics, Canada. Data are corrected for deadtime (spectrometer delay in the A/D converters) and normalized to cps (counts per second). Corrections for cosmic and aircraft backgrounds were made by using data from the spectrometer background lines. All radiometric data were normalized to a hight of 250 feet using data from the radar altimeter. Stripping was carried out to remove effects of spectral overlap. The values of the stripping ratios were calculated based on calibration measurements made prior to the survey. The data were gridded and filtered with a 7 by 7 Hanning filter before contouring.

4.4 Map products

The following maps have been generated at 1:50000 scale:

Map no. 93.046-01	Total magnetic field
-02	VLF, orthogonal channel
-03	VLF, inline channel
-04	Apparent resistivity, 4212 Hz
-05	Apparent resistivity, 4616 Hz
-06	Apparent resistivity, 34262 Hz
-07	Potassium counts per sec.
-08	Uranium counts per sec.
-09	Thorium counts per sec.
-10	Potassium:uranium ratio
-11	Potassium:thorium ratio
-12	Uranium:thorium ratio

Reduced versions of these maps in scale 1:131.000 are attached to the report.

4.5 Interpretation

Magnetics (Map 93.046-01): The total field magnetic map shows no correlation with either geological structure or stratigraphy. Magnetics therefore are not expected to be a useful aid to locating the alum shales. Nevertheless, the magnetics reveal a number of interesting features, attributed to the Precambrian basement rocks.

The granitic gneiss exposure at 6747000 N-633000 E exibits concentric low amplitude magnetic banding. To the north of this body, the mapped augen gneiss is characterized by strongly magnetized, and apparently shallow body at 6753000 N-631000 E. There are numerous similar magnetic highs in the area, making the granitic gneiss unit north of the mapped amphibolite unit significantly different from the gneiss located to the south of it.

In the south west of the survey area lies a series of 3 sub-parallel distinct lows striking at an angle of approximately 310 degrees. These lows might represent basement troughs, which deepen towards the south east. The northernmost of these lows lies over the course of Svartelva as it runs into Åkersvika. It could therefore represent a basement topographic low which also correlates with a low in the surface topography.

VLF-EM Maps (Maps 93.046-02 and -03): VLF measurements are sensitive to regional conductors striking in a direction towards the transmitting station. Because of this directional sensitivity, two VLF stations are selected when VLF measurements are done.

The Orthogonal VLF channel is dominated by three major linear features which strike approximately 30 degrees east of north, and which are associated with the carbon rich facies of the alum shales and north north-easterly trending faults created during Permian rifting. As VLF is sensitive to long regional conductors, and as the shale and the faults intersect, the source mechanism can switch between the two.

Over much of the survey area covered by sediments, many of the weaker orthogonal VLF anomalies can be attributed to cultural features, such as power lines or water supply pipes. There are numerous small anomalies that cannot be attributed to cultural effects however, and these may reflect the presence of small alum shale outcrops or fractured bedrock.

The inline VLF map is sensitive to features which strike across the strike direction of the alum shale outcrops and Permian faulting. This map reveals few features which are worthy of note.

Apparent Resistivity Maps (Maps 93.046-04, -05 and -06): Apparent resistivities over parts of the Undifferentiated Series are quite low. These areas coincide with the VLF conductors, and are interpreted to be to the carbon rich facies of the alum shales. As in the VLF, three distinct conductive bands are seen, each striking roughly parallel at approximately north 30 degrees east. The crystalline basement is mapped as being extremely resistive, and units within the basement cannot be differentiated on the basis on resisitivity alone. Intermediate resisitivities are generated for remaining sedimentary cover units, with the resistivity of the Hedmark group being greater than that of the Cambro-Ordovician deposits.

Higher frequencies penetrate into the ground less distance than lower frequencies do, so resistivity data from several frequencies can be used to build a picture of the resitivity distribution in the ground as a function of depth. The 34262 Hz apparent resisitivity maps shows the units interpretated to be the conductive alum shales to be both thinner and to be lying on the east side of the similar resistivity lows on the 4218 Hz apparent resistivity map. Thus alum shales are inferred to be dipping gently to the west north west in a direction roughly orthogonal to their trace on the surface. The increased breadth of the anomalies at low frequency relative to their breadth at high frequency is interpreted to mean that the conductive shale facies is covered by non-conductive facies in the Undifferentiated Series as it dips away from the surface. This dip probably represents a general regional tend which is punctuated by Permian faults.

The westernmost conductor extends west of the granitic basement outlier east north-easterly to the mapped contact of the Stein Formation with the Undifferentiated Series. The low resistivity anomaly weakens as it continues north from this point, perhaps an indication that the conductor continues under the limestone cover. The western extent of the anomaly correlates well with the mapped location of a Permian fault.

The central conductor attributed to the carbon rich shale facies runs roughly along the contact between the sedimentary cover and the granitic basement from Romedal, through Adalsbruk and Løten. The conductor then continues northward from Løten to 6755000 N-630000 E along a trace which does not conform either with contacts or faults on the geological map, but which is interpreted to be a continuation of the alum shale outcrop. This continuation is also seen in the VLF orthogonal channel. Discontinuities in the conductor correlate well with the granitic fingers near Romedal and Adalsbruk.

The eastern conductor attributed to the carbon rich shale facies runs subparallel to the central conductor, and correlates well with the finger of Undifferentiatesd Series running southward from 6747000 N-629000E. The conductor is quite distinct from approximately 6742000 N, and extends well north of the mapped extent of the Undifferentiated Series, again an indication that the shales extend north and east of their mapped extent. This extension of the conductor north of the Undifferentiated Series is also seen in the VLF orthogonal channel.

This linear pattern of conductivity is broken near the south east corner of the survey area, with the break associated with the location of the strong magnetic lows. Again, the high frequency resistivity anomalies cover less area than the low frequency anomalies, indicating the shales extend to depth. The pattern of electrical conductivity in this area is rather complicated, perhaps an indication that the conductor here has been heavily deformed.

Potassium (Map 93.046-07): The potassium map shows many of the features of the uranium map (see discussion following) but with diminished sensitivty, indicating the uranifferous zone of the alum shales is elevated in potassium in comparison with the rest of the units present in the Løten map sheet.

Uranium (Map 93.046-08): There is considerable coincidence of uranium anomalies and electrical conductors defined from the apparent resistivity, supporting the hypothesis that the helicopter electromagentic system is mapping uranifferous alum shale facies. The excellent correlation of the uranium channel with the geologic boundary between the Undifferentiated Series and the Precambrian basement, and with low resistivites, indicates that the uranium sources are either from bedrock sources or that overburden has only been marginally displaced by glacial transport.

Uranium anomalies also extend significant distances from the electrical conductors, and in directions which are not consistent with ice transport. A possible explanation for this is that a uranium rich facies exists which does not correlate with the conductive carbon rich layer.

The northern extent of the uranium 20 count/sec contour correlates well with the mapped southern extent of the Bjørge Formation north of Hamar, suggesting this formation acts as a cap rock which has pervented uranium and/or radon from appearing at the surface. The distribution of uranium south of this point is considerably more complex than the geological map would suggest. This would indicate that either the Stein Formation is also a source of uranium, or that revisions to the geological map may be necessary.

Thorium (Map 93.046-09): The thorium map exhibits many of the same characteristics as the potassium map, and is not particularly noteworthy apart from the fact that the highest thorium values tend to occur in the southwest part of the survey area.

Potassium Thorium Ratio Map (Map 93.046-10): The potassium thorium ratio is dominated by a relative increase of potassium relative to thorium progressivly eastwards, and this relative low in potassium to the west might be due Bjørges formation. Nevertheless, this general trend is interrupted by a series of north south trending highs which do not correlate well with other geological or geophysical features. The eastern most conductor associated with the carboniferrous shales of the Undifferentiated Series is distinguished by a low potassium-thorium ratio. Similar correspondance with conductors at other locations on the map is however difficult to justify.

Potassium Uranium Ratio (Map 03.046-11): The potassium uranium ratio map is domianted by the distribution of uranium, and bears strong respelances to the uranium count map. The granite gneiss located at 6747000 N-631000 E is characterized by a relatively low

ratio in contrast with the remainder of the Precambrian units, and the extension of the eastern most conductor towards the north of the map can be traced by a slight low in the ratio.

Uranium Thorium Ratio (Map 93.046-12): On the basis of the granitic thumb at 6741000 N-624000E, the window centered at 6741000 N-621000 E, and the eastern extent Undifferentiated Series formation, count ratios of approximately 2 in the uranium thorium ratio correlate well with the extent of the Undifferentiated Series. High ratios are also associated with the magnetic lows and apparent resistivity anomalies where Svartelva runs into Åkersvika. If this low is a result of basement depth variation, this depth variation may control the amont of shale exposed at the surface there and thus the relative abundance of uranium.

5 THE GROUND FOLLOWUP SURVEY

Radon in the ground can exist either in a gaseous phase in the soil pore spaces, in which case it may be free to migrate to the surface, or bound within a crystal lattice where it remains immobile. Gamma ray measurements on their own cannot distinguish between the free and bound states, but instead measure total soil radon content. The purpose of the ground followup then, was to develop an understanding of the relative partitioning in the soil of radon in the free and bound states, and consisted of ground radiometric and soil gas samples along profiles following the helicopter traverses.

5.1 Ground Radiometric and Radon in Soil Measurements

The ground radiometric measurements served two major purposes. Firstly, they could be used to establish a direct comparison with the airborne measurements, and thereby verify the ground survey was correctly positioned. Secondly, soil gas concentrations are expected to vary substantially on a scale over which a single airborne measurement can only provide an average measurement. Combined ground radiometric measurements and soil gas data therefore provides the connection for linking airborne gamma ray measurements to radon gas availability in the ground.

To minimize variation due to seasonal and meteorological effects, ground followup measurements were made withing two weeks of the helicopter survey. Measurements were made along three lines following selected segments of the helicopter profiles. Followup line locations were chosen after a preliminary analysis of the analogue data records, and without the benefit of the map products which have been subsequently generated. Each line took approximately 1 day to complete.

The ground measurements were taken at stations separated by 50 meters, and consisted of three measurements of local gamma ray activity and two samples of radon gas from holes approximately 40 cm deep. The gas samples were taken at separate points, approximately 50 to 100 cm apart. The gamma ray measurements were taken with an Exploranium GR-256 cesium stabilized spectrometer by suspending the sensor approximately 30 cm above the ground. At each station, three points separated by approximately 3 meters were measured, each for a duration of 2 minutes. A schematic diagram illustrating a typical sampling configuration is illustrated in Figure 7.

Soil gas measurements are tricky, since any measurement invariably requires a disturbance of the soil, and thus the possibility of changing the local concentration of the soil gas. One must

be careful to compact the soil on the sides of the hole in a reasonably consistent manner to permit consistent infiltration of soil gas, and take care not to ventilate the soil with too much fresh air. For a more thorough description of the sampling problems associated with radon gas measurements in soils, refer to Tanner (1991) and Duval (1990).

Two methods of radon measurement are possible; an instantaneous, or grab sample measurement, and a time averaged measurement. Time averaged measurements are typically made with etched-track film left in the ground for periods of a week or more, and are less susceptible to temporal variations in ground radon content introduced by meterological effects than are measurements made instantaneously. Instantaneous measurements have the advantage that it is only necessary to occupy sampling site, and were used for the followup work described here.

An EDA portable emanometer was used for the gas sampling . The emanometer measures radon from a hole in the ground by cycling the soil gas from the hole, through a zinc sulphide scintillation chamber, and back to the hole again. The gas is pumped with a hand bulb from a tube extending to the bottom of the hole, through the chamber, and is then returned back again at the top of the hole. Once the air has been circulated through the instrument, the activity of the gas in the scintillation chamber is measured for a fixed period of two minutes.

To make the holes required to extract the gas samples in this study, a steel wrecking bar with a blade on the end was used. A consistent technique for creating the hole was finally developed by the third (and last) day of field work, in which the holes were made by driving the bar vertically into the ground with approximately the same force on every stroke, to ensure soil compaction on the sides of the hole was relatively consistent. The blade was rotated approximately 60 degrees on every stroke until a hole of sufficient depth was excavated. The bar was never withdrawn from the hole by exerting enough lateral force to move the bar at top of the hole a distance of more than 3 cm. This was done to avoid making horizontal cracks in the soil at the base of the hole which if opened and closed through the lateral motion of the bar, could ventilate the soil with outside air. Where the ground proved to be too stony to generate a hole of sufficient depth using this technique, the hole was abandoned in favour of a different site.

Once a hole had been excavated, it was covered with a plastic cap for approximately three minutes before the EDA soil gas probe was inserted and air circulated between the hole and the instrument sensor chamber. A fixed amount of air, determined by 5 pumps of the bulb pump of the intake to the scintillation chamber were made in each case so as to acheive consistent results. Prior to each measurement, the scintillation chamber was purged with fresh air and an instrument background measurements was taken.

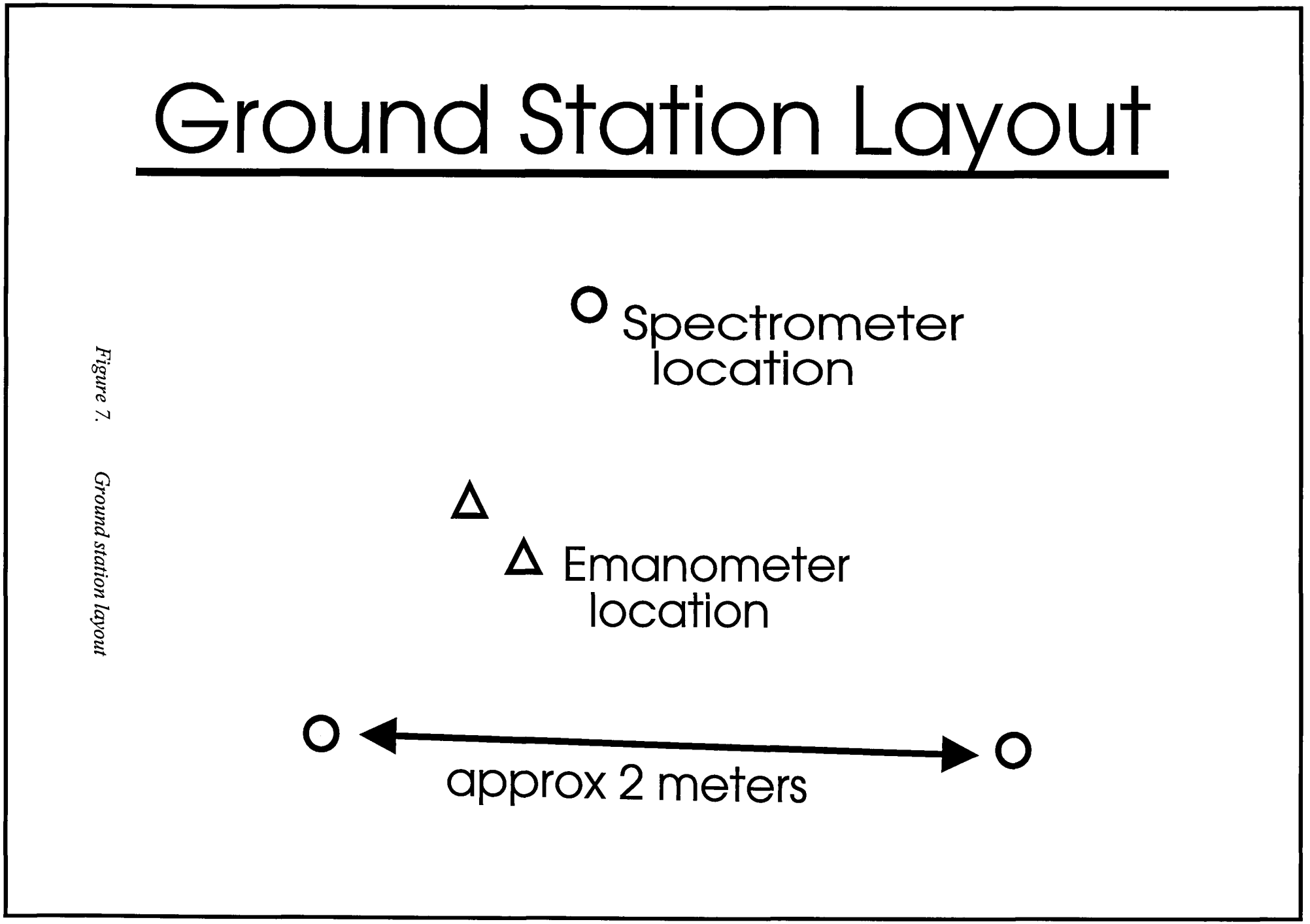

Figure 7. Ground station layout

The scintillation cells can become contaminated with the short lived by decay byproducts of radon gas, particularly if they are used where to measure active gas samples. As such it is advisable to carry along at least 5 or 6 chambers during a survey. The chambers should be flushed with fresh air following every measurement, and checked for constant (non decaying) background values prior to every measurement. Difficulty was encountered in this regard on the second day of surveying , where particularly active samples were measured since only 2 chambers were present in the field for measurement. Backgrounds became so high and variable that it was impossible to reliably measure weakly active soil gas samples.

A number of factors, such as soil porosity and permeability, dampness and homogeneity can introduce variations in the soil gas measurement, and these variations can exist on quite a local scale. Nevertheless, the results obtained on the third day indicate that despite the problems inherent in soil gas measurements, consistent results are possible if sufficient care is taken when the samples were made.

5.2 Ground Survey, Results and Analysis

Of the three days sampling effort, I consider that only the results from the third day to be reliable. The holes made during the first two days were not made in a repeatable systematic fashion, and data collected on the second day suffered problems with highly active cells and thus unreliable background measurements.

The profile measured on the third day roughly followed 6746000 N, from approximately 618000 E to 619000 E, and is shown in figure 8. Stations were separated by 50 meters, and were located in cropped, cultivated fields. Soil characteristics were judged to be constant over the profile, with no particularly large changes observed either in the stoniness, composition or moisture content. Such uniformity would be expected to contribute to the consistency of the soil gas measurements.

Before analysing the ground followup data backgrounds were stripped from each gas sample measurement, and gas sample data were sorted into minima and maxima for each station. The radiometric data were corrected for Compton scattering but no backgrounds were removed.

Uranium and thorium radiometric data, and radon soil gas data are plotted in figure 9.

Results indicate that the uranium and radon gas data correspond well, with highs in the radon data at stations -2,3 and 8 corresponding with highs in the uranium profile (Figure 8). Correspondence between the thorium data with the uranium and radon data sets is much

weaker (Figure 9), with the thorium variation relative to the thorium background being much weaker than the variation in the other two data sets. There is a slight elevation in the thorium level at stations -2 and 3 corresponding to the radon and uranium peaks. The correlation in the peak position may be related to improved gamma-ray signal resulting from a reduction in soil moisture content or other local variations affecting the strength of the gamma-ray signal.

The soil gas and ground spectrometer data were then used to establish a relationship between soil gas and gamma ray measurements. To do this, radon gas readings were plotted as a function of uranium -thorium ratio along the profile, with the ratio being chosen to mitigate the effects of local variability on the gamma-ray signal. Results are shown in figure 10, with a best linear fit, and while the results are not good enough to predict with certainty that a particular ratio will yield a specific gas reading, a definite tend between the likelihood of a high radon soil gas reading increases with the uranium-thorium ratio. In this sense, these results corroborate those of a similar radon soil gas by Duval (1990, Figures 24 and 25) and a study of free radon in Ohio Shales by Harrell et. al (1991, Figure 4); the statistical variation in all studies appears to be similar. It is not possible however to state the fraction of radon available as soil gas as no relative calibration between the emanometer and the portable spectrometer has been made. The rise in spectrometer count rates associated with the presence of soil gas may be due entirely to free gas in the pore space of the soils, but this is doubtful. Although some increase in spectrometer count rate is likely due to free soil gas, some is undoubtably due to the presence of the shale itself in the overburden.

Finally, a link between the ground and airborne radiometric data is made in figure 8. The airborne data shown in the figure were extracted from the database prior to line filtering operations but after the Compton correction stage, so as to minimize any spatial variation at the detail required for this comparison. Results of the comparison are excellent, with peaks in both data sets coinciding. Width of the peaks in the airborne data set are considerably wider than are the peaks in the ground data, and this increased width is a result both of the higher airborne sensor altitude as well as from its lateral displacement during each measurement cycle. The airborne sensor would measure an area approximately 150 by 120 meters during each measurement. In contrast, the ground measurement would be sensitive to variations on the order of a few meters, and since measurements were made at 50 meters intervals, ground station variation would be of this order. Since the airborne radiometric data correlate well with the ground data, then because of the correlation between the ground radiometric and radon data, one would thus anticipate that the airborne data are sensitive to the presence of free radon gas in the soil. Given this result, one would expect, therefore a further correlation of airborne uranium data with radon measurements in dwellings as was reported in work cited by Neilson et. al (1991).

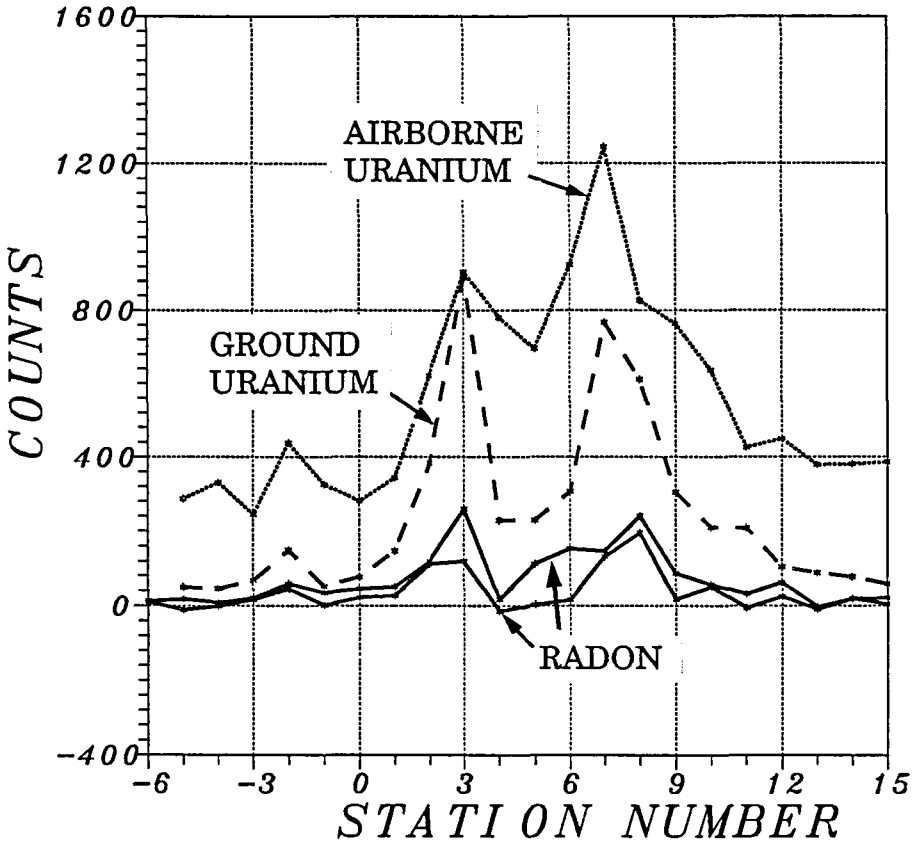

Figure 8. *Airborne, ground and radon data from the follow-up profile, day 3*

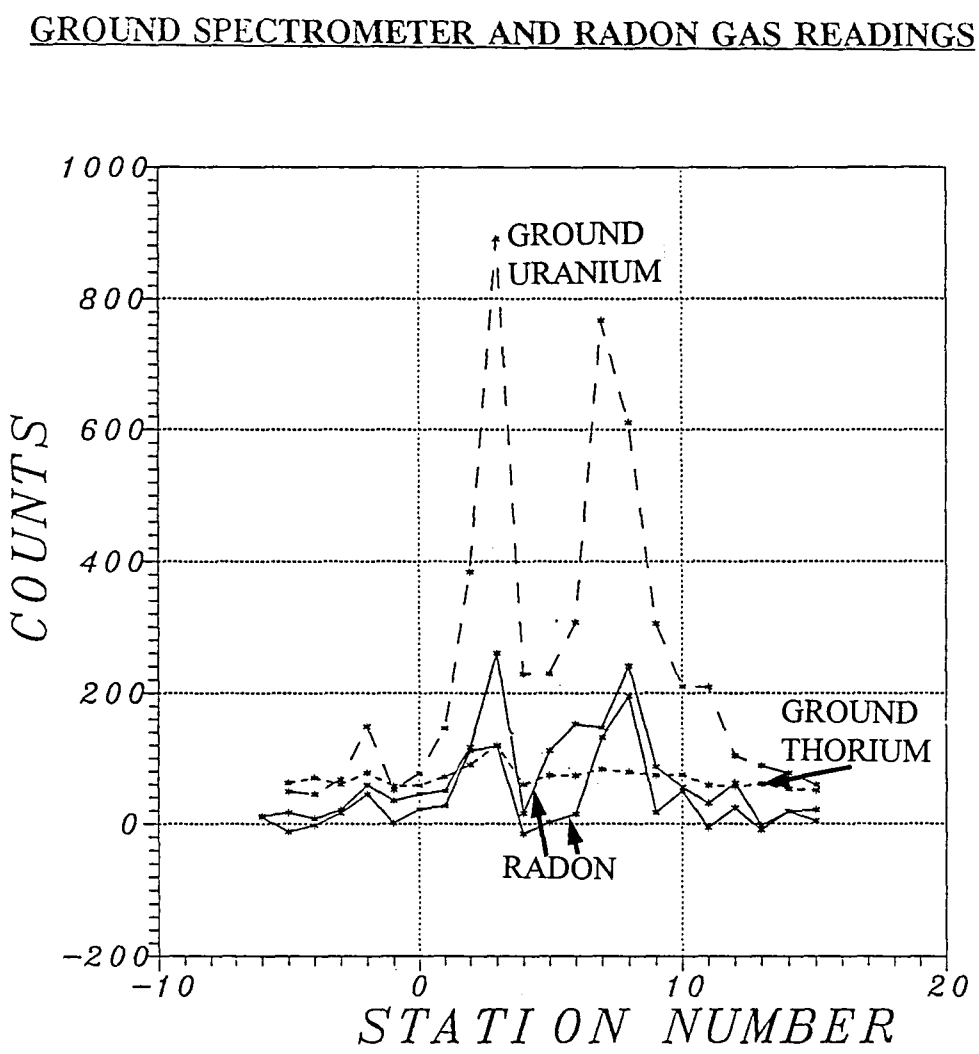

Figure 9. Ground uranium, thorium and radon data from the follow-up profile, day 3

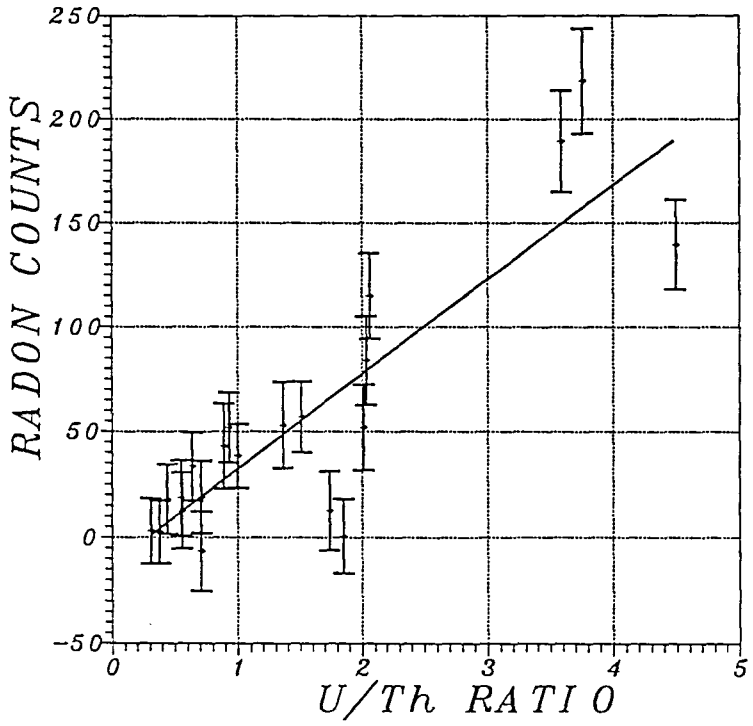

Figure 10. Radon vs. ground uranium/thorium ratio

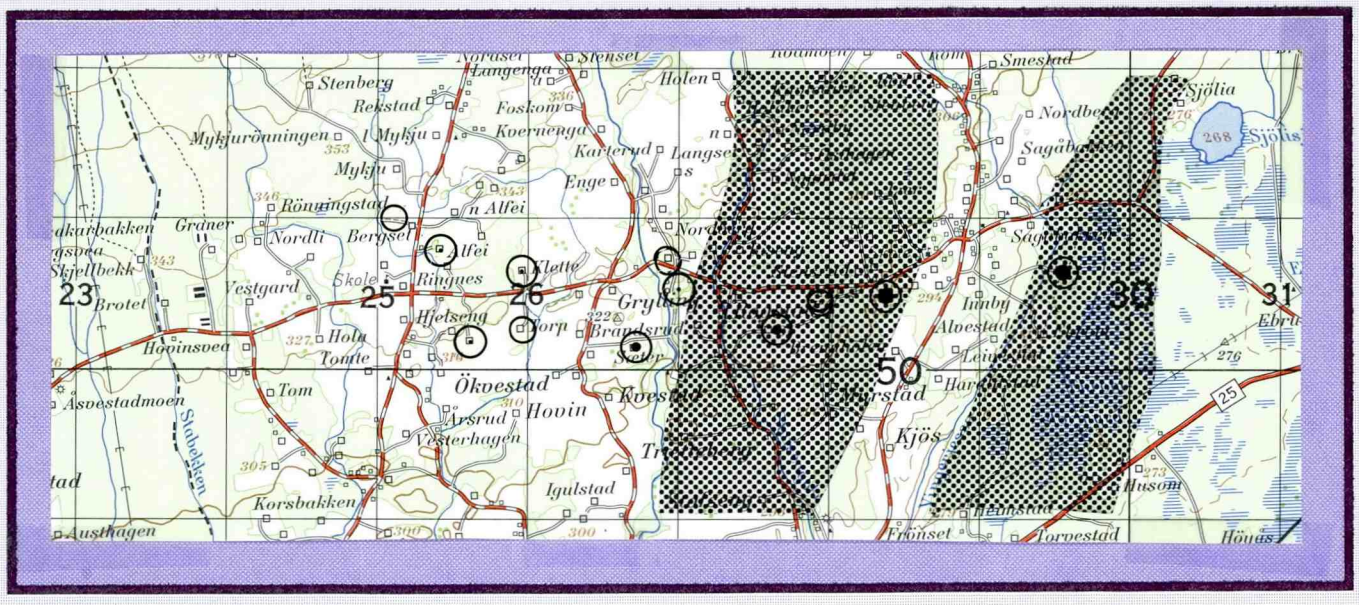

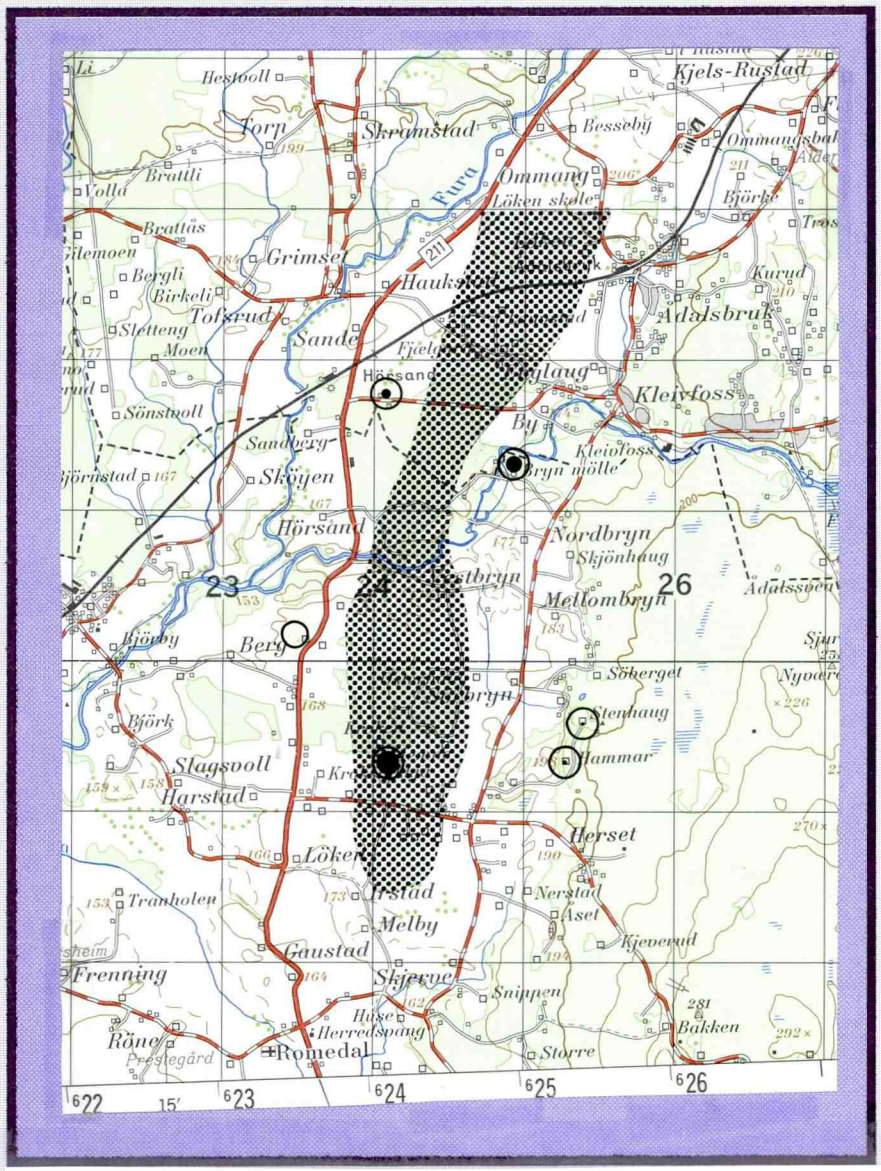

RADON IN WATER

Radon

0-14 ○

15-24 ⊙

25-49 ⊙

50-74 ◉

> 75 ◉

Conductor

Figure 11. Radon in water (kBq/m^3) plotted with interpreted EM conductors

5.3 Airborne Radiometric Data & Radon in Dwellings

To test the hypothesis that airborne radiometric data could be used as a basis for assessing the risk associated with indoor radon gas concentrations, radon concentration and exhalation data measured in the Løten area by Statens strålevern were compared to the gridded airborne uranium channel. The data initially provided by Statens strålevern were compiled by address, and could not be easily converted into geographical location for comparison with the gridded data. Instead, a map of indoor concentration and exhalation rate prepared by Løten kommune in which concentration and exhalation data were plotted as symbols at the locations where those data were acquired. These data are summarized in Appendix 1.

The map prepared by Løten kommune was not ideal for this study for two reasons. One was that the symbols were large and center points could only be recovered with an accuracy of 100 meters at best, and so introduced errors when correlated with the gridded data. The second was that the results were grouped into broadly defined data ranges, thus eliminating the possibility of generating a correlation coefficient between the two data sets. So a contingency table analysis was used.

Contingency tables are used to compare two binned data sets, and are a tabulation of the number of occurrances in a bin of one data set against the number of occurrances in bins of the second data set. To build the contingency table, it was thus necessary to bin the corresponding airborne uranium data set into discrete ranges. This was done using bins in the range of 0-50, 51-75, 76-100 and over 100 cps. Contingency tables were thus generated for count rate against exhalation data and count rate against concentration data, and are presented as tables 1 and 2.

Analysis of the exhalation contingency table shows a strong diagonal trend, with accumulated totals lying on the table diagonals or adjacent to them being considerably larger than more accumulated totals with a greater separation. This is interpreted to support the inference that the airborne measurements are sensitive to radon gas in the ground, which in turn are positively correlated with exhalation of radon gas into homes. The link between the concentration data and the airborne uranium data is less strong, likely because concentration data are more relatively dependent on building construction and operation (including unaccounted for seasonal effects and the nature of the water supply) in comparison to the abundance of radon in the ground than are exhalation data. The correlation, however, is still positive, indicating that an increase in the uranium count rate can be associated with a increased probability of radon gas concentrations in houses.

Table 1:Radon Exhalation vs. Airborne Uranium Counts

	URANIUM CHANNEL (COUNTS/SEC)				
RADON EXHALATION (Bq/m^2h)	RANGE	0-50	51-75	76-100	>100
	0-200	4	0	0	0
	201-400	2	0	0	1
	401-1000	0	0	2	1
	>1000	1	1	5	7

Table 2: Radon Concentration vs. Airborne Uranium Counts

	URANIUM CHANNEL (COUNTS/SEC)				
RADON CONCENTRATION (Bq/m^3)	RANGE	0-50	51-75	76-100	>100
	0-200	4	1	2	1
	201-400	10	5	0	0
	401-1000	6	3	0	2
	>1000	0	2	0	4

The results obtained in this study thus positively link the occurance of radon gas in houses with airborne geophysical measurements. However, it is possible that by more accurately locating the sites where the exhalation and concentration measurements were made, the correlation with the airborne radiometric data could be further strengthened.

Nevetheless, airborne uranium levels of 50 cps or more are associated with 85% of the sites with an exhalation rate of 200 $Bq/m^2/h$ but only half the sites with concentrations of site with concentrations of more than 200 Bq/m^3.

5.4 Analysis of the Radon in Water Data

To investigate the possibility of using airborne geophysical measurements to investigate the occurrance of radon in the ground water supply, samples of well water taken from local farms were analysed for their radon content and compared with the geophysical data. The initial sampling pattern, planned prior to field work, had to be drastically altered as the kommune had recently installed a new water supply network in the area initially considered to be the most prospective for producing good results. In fact, in the sampling pattern that was subsequently improvised, it was discovered that most dwellings built over the shale as defined by the electromagnetic data were coupled either with the water supply network or used cisterns, because the ground water there has a foul sulpherous taste.

The presence of sulpher in the alum shales thus had an unexpected effect on this study. Since the sulpher produced a foul taste, people would naturally find alternate sources of water supply in such cases, either brooks, cisterns, or the municipal water network. Thus in the course of collecting water samples, it was difficult to find wells directly over the shales as mapped by the electromagnetics, and the use of wells for water supply was virtually predictable for the electromagnetic data alone. The resulting sampling is biased towards sites located away from the alum shale with a resulting sampling bias against high radon in water values. The results of this survey therefore do not provide unambigouos evidence for the association of elevated radon water gas levels with conductive horizons.

Appendix 2 describes the methodology used to collect the samples, and a listing of results. Water concentration data were then correlated analysed using the contingency table method against airborne radiometric and resistivity data. This analysis however, did not produce interpretable results for two major reasons. Firstly, water supply and filtration equipment tended to quite variable and could have affected radon concentrations. Secondly, many of the prospective sites over the interpreted locations of the schists were not serviced by wells and thus could not be sampled, so prospective sites with high radon concentrations are sparse.

Results which tend to corroborate the correlation of radon in water with electromagentic conductivity nevertheless were obtained. In figure 11, radon in water readings are plotted on a interpretation map showing conductor location interpreted from the electromagnetic data. The upper figure illustrates a profile taken along an east-west road running over conductors to the north of Løten, and the lower figure the initially planned study area. Elevated radon in water concentrations are observed in the vicinity of the conductors, with the highest values tending to be directly associated with the presence of a conductor. However, it is possible to find readings greater than 25 kBq/m^3 at distances of upto 500 meters from inferred conductors. It is also possible to find relatively low readings directly over the conductors.

Hypothetically, the association of uranium and carbon should mean that radon in ground water can be predicted from the electromagnetic data. As validation of the hypothesis, one should expect either high and low values of radon gas to be associated with conductors, with lower values found away from the conductors. This is in fact what was seen, but sampling problems meant that too few samples could be taken where gas concentrations were expected to be high to meaningfully support the hypothesis.

6 CONCLUSIONS

Airborne geophysics proved to be a success in mapping major and minor occurrances of the alum shale in the Løten area. The association of uranium with high organic carbon contents in the alum shales allowed radiometric measurements to be used in conjunction with electromangetic methods. Geological maps at 1:50000 scale are only of marginal use in such applications, as experience from this survey has shown that the distribution of uranium can be significantly different from that which would be expected from examining the geological map alone.

A correlation of radon soil gas with ground and airborne uranium channel measurements has been established. Radiometric measurements, based on a contingency table analysis of data provided to NGU by Statens strålevern, effectively outlined areas with high radon exhalation rates, and can be used to identify areas which have a high likelihood of elevated indoor radon gas concentrations. The implication of this is that airborne geophysical maps can be used to identify areas where additional preventative measures should be incorporated into buildings to prevent the entry of radon gas.

On a more local scale, detailed airborne interpretation can be used to identify areas where minor occurrances of shales occur, and such an occurrance was encountered on the ground follow-up line. Where this is the case, simply moving building sites by 50 meters can dramatically reduce the chance of having significant radon gas accumulate in a building.

Although the electromagentic (and VLF-EM) technique proved to be effective at locating alum shales, the concentration of radon in well water could not be effectively correlated with the electrical conductivity of the ground. However, as a general trend, it was noticed that the highest concentrations of radon in well water coincided with, or were close to, large conductors. It should be further pointed out that samples were biased away from dwellings that occurred on the conductors, and that this sampling bias could be predicted from the electromagnetic data.

The airborne data also proved to be a useful adjunct to the bedrock map, and has revealed several new magnetic structures which were not previously seen. The electromagnetic conductivity maps may also proved to be useful for refining the location of several geological contacts.

7 ACKNOWLEDGEMENTS

In a multidiciplinary study such as this one, credit must be shared with many people. The initial idea for this work in due to Henrik Håbrekke, who also managed to provide funding for it. Field work was carried out in three phases with John Mogaard during the first airborne acquisition phase, Torbjørn Sørdal during the ground radiometric and radon gas measurements phase and Torleif Lauritsen during the water sampling phase.

Thanks are also due to Bjørn Lind and Terje Strand at Statens strålevern for their assistance in providing radon concentration, emanation data and for processing our water samples. David Gee provided the author with copious background material on the alum shales in Scandanavia, the author's interpretation of which has been proofed by Connall MacNiociall.

Helikopterteneste A/S generously subsidized this work, and thanks are due to Leif Huus for expertly handling the aircraft and equipment during the airborne survey.

8 REFERENCES

Andersson, A., Dahlmann, B., Gee, D. and Snæl, S. 1983: Kerogen and uranium resources in the Cambrian alum shales of the Billingen-Falbygden and Næarke areas, Sweden, Geologiska Føreningens in Stockholm Førhandlingar, vol 104, pt 3, p 197-209.

Andersson, A., Dahlmann, B., Gee, D. and Snæl, S. 1985: The Scandinavian Alum Shales, Sveriges Geologiska Undersøkning, Nr 56 Ser Ca.

Bjørlykke, A., Høy, T. and Skålvoll, H. 1980: LØTEN berggrunnsgeologisk kart 1916-I M 1:50 000, Norges Geologiske Undersøkelse.

Bjørlykke, K. 1974: Depositional History and Geochemical Composition of Lower Paleozoic Epicontinental Sediments from the Oslo Region, NGU Bulletin 305.

Brookins, D.G. 1991: Correlation of soil and uranium with indoor radon in the Albequerque N.M. area, Env. Geol. and Water Sci., 17, 209-217.

Cui, L.P. 1990: Radiometric methods in regional radon hazard mapping, Nuclear Geophysics 4, p353-364.

Duval, J.J. 1990: Soil gas radon compared to aerial and gamma ray measurements at study sites near Greely and Ft. Collins, Co., USGS Open file report RN:90-0648.

Follestad, B.A. 1973: Beskrivelse til kvartærgeologisk kart 1916 I - M 1:50 000, NGU Nr. 296, Universitetsforlaget.

Foslie, S. 1919: Kulskiferen ved Gjøvik, Tidsskrift for Bergvæsen 7, nr 3.

Gee, D. 1980: Basement cover relationships in the central Scandinavian Caledonides, Geologiska Føreningens in Stockholm Førhandlingar, v 102, pt4, p 455-474.

Gregg, L.T. and Holmes, J.J. 1991: Radon detection in soil and groundwater, Geotechnical and environmental geophysics, Investigations in geophysics 5, p 251-262.

Harrell, J.A., Belsito, M.E. and Kumar, A. 1991: Radon hazard associated with outcrops of the Ohio Shale in Ohio, Environmental Geology and Water Sciences, 18, p17-26.

Martinez, L.A. and Palomares, J. 1991: On the determination of 226Rn in soils and uranium ores by direct gamma ray spectrometry, journal of Radioanalytical and Nuclear Chemistry, 147, p 225-234.

Nazaroff, W.W. 1992: Radon transport from soil to air, Reviews of Geophysics, 30, p 137-160.

Neilsen, D.L., Cui L.P. and Ward, S.H. 1991: Gamma ray spectrometry and radon emanometry in environmental geophysics, Investigations in Geophysics, 5, p 219-250.

NGU 1967a: Radiometrisk kart, 1916 I Løten. Norges geologiske undersøkelse.

NGU 1967b: Aeroelektromagnetisk kart, 1916 I Løten. Norges geologiske undersøkelse.

Olerud, S. 1980: Oppfølging av bakkesedimentanomalier på Romeriksåsene, NGU Rapport 1650/49c.

Olerud, S. 1982: Elsjøfeltets geologi, tektonikk og innhold av sporelementer i kambro-ordoviciske skifre, NGU Rapport 1650/16d.

Olerud, S. 1984: Metallogeny of the Elsjø area, northern Oslo region, Norway, Norsk Geologisk tidsskrift, vol 64, p 325-334.

Rose, A.W. and Hutter, A.R. 1990: Sampling variabilty of radon in soil gasses, J. of Geochem Expl., 38, p 173-191.

Rose, A.W., Hawkes, H.E. and Webb, J.S. 1979: Geochemistry in Mineral Exploration, Academic Press.

Singh, M., Ramola R.C., Singh, S. and Virk, H.S. 1990: Influence of moisture content on radon diffusion in soil, Nuclear Geophysics, 4, 479-482.

Skjeseth, S. 1958: Uran i kambrisk alunskifer i Oslofeltet og tilgrensende områder, NGU Årbok, p 100-111.

Statens Institutt for Strålehygiene, 1991: Radon i boliger, Østerås Norway 778.

Tanner, A.B. 1991: Error in measuring radon in soil gas by means of passive detectors, Nuclear Geophysics, 5, p 28-30.

Appendix 1

CONTINGENCY TABLE DATA

The following table lists the data used to create the contingency tables 1 and 2. The eastings and northings are the approximate centers of the symbols on the map shown following on page. This map was created by Løten kummune, and provided to NGU by Statensstrålevern. Corresponding concentration and exhalation data are the ranges indicated by each symbol. The uranium data were obtained from the gridded helicopter data, at points located at the corresponding symbol center location. N/A means not analysed.

Reading	UTM East	UTM North	Concentration (Bq/m^3)	Exhalation ($Bq/m^2/hr$)	Uranium Counts
1	624075	6743550	0-200	N/A	27
2	623900	6743950	N/A	400-800	79
3	625500	6743300	N/A	>1000	96
4	625700	6743100	400-1000	N/A	50
5	627500	6740150	400-1000	N/A	22
6	628650	6741800	N/A	0-200	13
7	628200	6742600	200-400	N/A	46
8	630075	6743850	400-1000	N/A	13
9	629650	6743950	N/A	200-400	16
10	628450	6744300	>1000	N/A	66
11	628550	6744550	N/A	>1000	110
12	629000	6744550	200-400	N/A	58
13	628925	6744950	N/A	>1000	82
14	629075	6745400	>1000	N/A	67
15	629150	6746100	N/A	>1000	93
16	629250	6746400	400-1000	N/A	72
17	626000	6744150	>1000	N/A	128
18	626500	6744100	N/A	>1000	107
19	625950	6744450	N/A	>1000	80
20	627100	6744550	N/A	>1000	47
21	625750	6745200	N/A	>1000	116
22	626750	6745125	400-1000	N/A	23
23	627300	6745000	N/A	200-400	39
24	627675	6745150	N/A	0-200	32
25	628725	6745350	0-200	N/A	75
26	628300	6745650	0-200	N/A	120
27	628550	6746000	0-200	N/A	73
28	627850	6745950	200-400	N/A	42
29	627450	6745900	200-400	N/A	63
30	626900	6745500	200-400	N/A	39
31	625750	6745250	N/A	>1000	125

Continued on the following page .....

Concentration, exhalation and count rate data continued from the previous page:

Reading	UTM East	UTM North	Concentration (Bq/m^3)	Exhalation ($Bq/m^2/hr$)	Uranium Counts
32	623600	6746250	200-400	N/A	23
33	625200	6746275	400-1000	N/A	36
34	625600	6746600	200-400	N/A	30
35	625650	6746100	N/A	>1000	59
36	625950	6746300	0-200	N/A	87
37	626100	6746700	400-1000	N/A	30
38	626400	6746350	0-200	N/A	74
39	625550	6746400	0-200	N/A	38
40	627500	6746500	>1000	N/A	119
41	627700	6746750	N/A	>1000	102
42	626400	6746800	200-400	N/A	25
43	626950	6747000	400-1000	N/A	153
44	624200	6747400	400-1000	N/A	23
45	624600	6747450	400-1000	N/A	63
46	624500	6747800	N/A	200-400	106
47	624800	6748075	N/A	>1000	97
48	626550	6747600	200-400	N/A	35
49	628500	6747500	200-400	N/A	74
50	626150	6748050	400-1000	N/A	102
51	626800	6748150	>1000	N/A	146
52	625600	6748600	200-400	N/A	61
53	627200	6748800	>1000	N/A	184
54	628750	6748600	N/A	0-200	16
55	627200	6749050	N/A	400-1000	115
56	624950	6749800	200-400	N/A	38
57	628150	6749700	200-400	N/A	43
58	625350	6780100	N/A	400-1000	74
59	626600	6750400	N/A	>1000	125
60	628800	6750750	0-200	N/A	25
61	626725	6750900	0-200	N/A	21
62	626750	6751100	N/A	0-200	20
63	627500	6751050	N/A	>1000	120
64	628800	6751675	0-200	N/A	5

The map from which the concentration and exhalation data were taken follows:

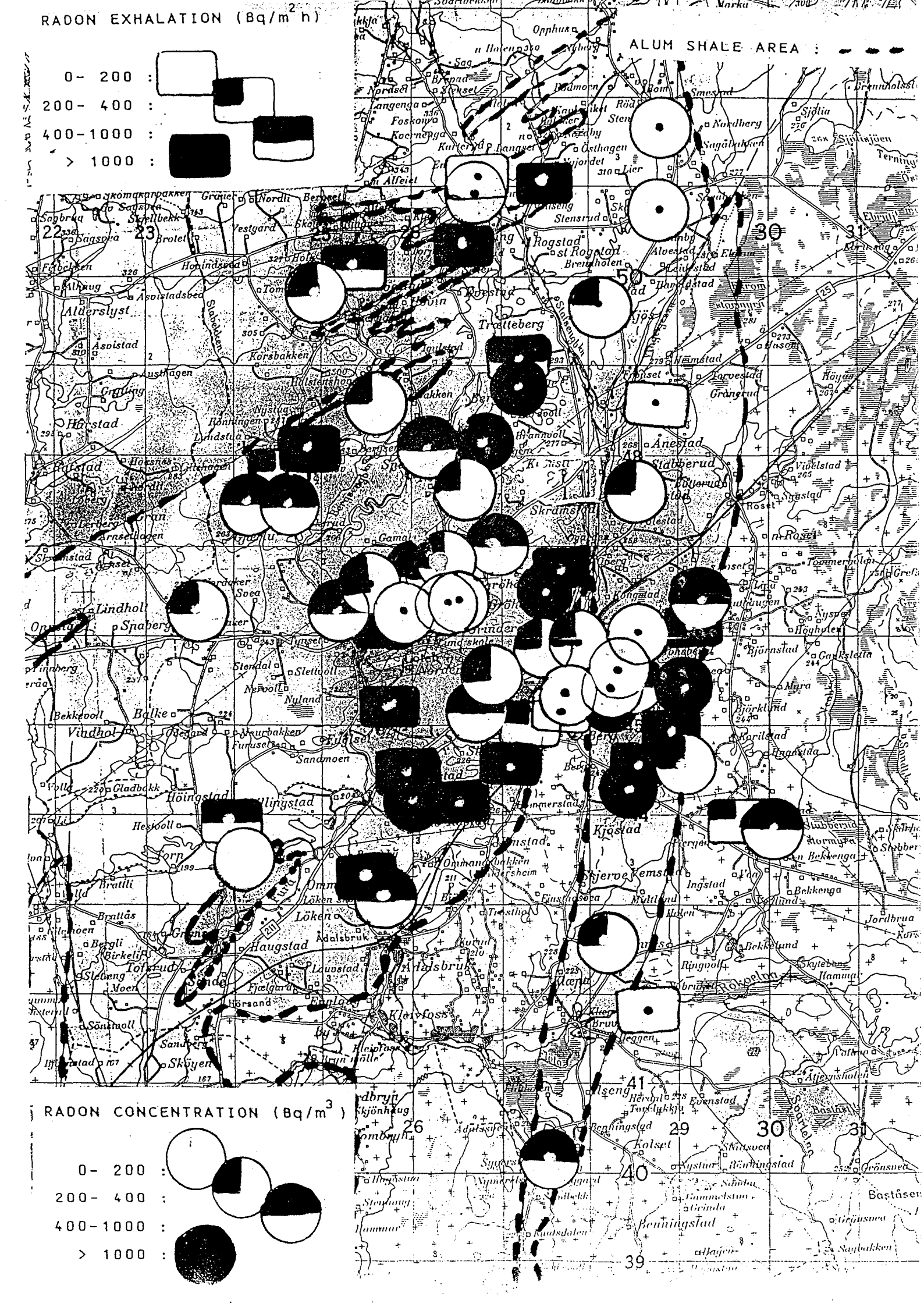
RADON EXHALATION (Bq/m² h)
0- 200 :
200- 400 :
400-1000 :
> 1000 :
ALUM SHALE AREA :
RADON CONCENTRATION (Bq/m³)
0- 200 :
200- 400 :
400-1000 :
> 1000 :

Appendix 2

RADON IN WATER MEASUREMENTS

Radon in water was sampled from the wells in the Løten area on August 16,17 and 18, 1993, one year following the helicopter measurements. Water samples were usually collected from taps inside dwellings, after the water had been allowed to run for approximately 5 minutes. Samples were drawn by inserting a pipette into a glass of water held under the tap such that no bubbling or turbulence occurred. The water samples were then inserted into a vial of scintellating gel and sent to Statensstrålevern by overnight courier for analysis.

The following table summarizes the results from the radon survey and the corresponding EM and uranium data processed from the helicopter survey. Each row represents data from one sample location, namely, its approximate position in UTM, the radon in water results in kBq/m^3, log (base 10) of the 4218 Hz apparent resistivity expressed in ohmm, the airborne uranium count rate at that location (in counts per second), and the name of the household from which the water sample was collected.

Sample	UTM-E	UTM-N	Radon	Resistivity	Uranium	Household
1	625350	6750800	12,4	-2.1	23	Ødegård
2	625150	6751050	12,0	-2.6	29	Dotterud
3	625560	6750200	22,0	-2.3	52	Evensen
4	626050	6750550	15,6	-2.1	40	Klette
5	625950	6750300	14,0	-2.2	47	Grøholt
6	626700	6750150	46,4	-2.0	145	Sæther
7	626900	6750750	8,7	-1.5	23	Reiersen
8	627050	6750550	13,0	-1.5	28	Sorprud
9	627900	6750450	13,1	-0.6	90	Bakken
10	628400	6750500	53,2	-0.3	48	Ramsøy
11	627600	6750250	26,8	-0.7	152	Flagstad
12	627650	6751250	19,3	-0.8	102	Johansen
13	627850	6751400	15,2	-0.7	15	Jensen
14	629150	6753500	15,8	-0.2	12	Østborg
15	628850	6753300	14,2	-0.9	9	Øvergård
16	628550	6753300	7,2	-0.9	9	Engebakken
17	626200	6752250	25,2	-2.1	12	Sømoen
18	626650	6752300	9,6	-1.8	7	Ytterøy
19	626600	6752450	27,8	-1.9	8	Haraldsen
20	627200	6752450	25,6	-0.9	17	Enger
21	628200	6752850	26,7	-0.5	18	Andrå
22	628300	6752800	7,8	-0.5	18	Grønstad
23	628300	6752900	15,8	-0.4	18	Grønstad
24	628300	6753100	12,5	-0.7	13	Slåttbakken
25	617500	6745950	8,0	-1.6	17	Bakken
26	617500	6745950	8,7	-1.6	17	Bakken
27	618400	6745700	13,8	-2.3	45	Hoelstad
28	618250	6746000	8,1	-1.8	27	Hagen

29	618900	6746850	17,4	-2.2	17	Kjøs
30	622950	6745750	7,7	-2.0	27	Pedersen
31	623000	6745500	24,0	-2.2	17	Sørli
32	622750	6745850	6,8	-0.9	50	Nybakken
33	622400	6746300	134,5	-1.1	55	Lindholt
34	621700	6747000	63,2	-2.0	33	Skramstad
35	622900	6746750	8,8	-0.6	43	Lindstad
36	621450	6745550	8,7	-1.2	35	Holte
37	624050	6739350	81,1	-0.6	65	Asbjørnsen
38	625250	6739300	23,3	-2.8	42	Oustad
39	625350	6739600	18,5	-3.5	27	Steinhaug
40	624850	6741300	58,9	-2.4	12	Løvlien
41	624000	6741800	26,1	-1.1	17	Sandergen
42	626850	6748050	29,9	-1.2	99	Haugen
43	627100	6748450	37,6	-0.9	115	Nordvold
44	630300	6751950	5,8	-0.7	12	Kallnes
45	630200	6752700	5,9	-1.7	8	Lien
46	630250	6752750	11,1	-1.8	8	Lien
47	630400	6753000	12,1	-1.6	13	Libak
48	629400	6753150	5,6	-2.4	8	Nybekken
49	627950	6751950	13,8	-0.7	9	Enger
50	629500	6750650	54,6	-0.7	48	Tømmerholen
51	623550	6740150	8,3	-1.4	36	Salveson

NORGES GEOLOGISKE UNDERSØKELSE
Geological Survey of Norway

MAP 01
TOTAL MAGNETIC FIELD

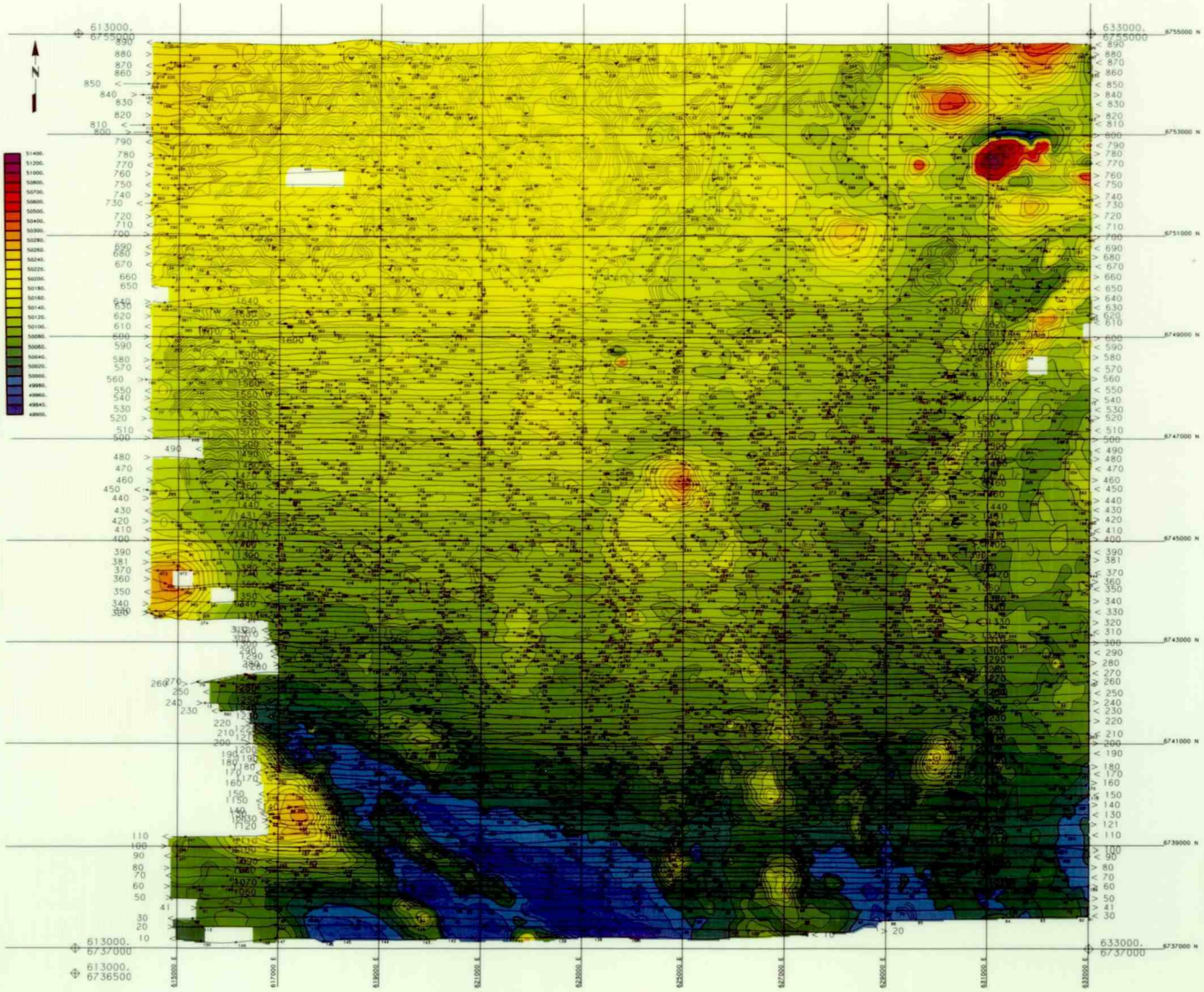

NGU
NORGES GEOLOGISKE UNDERSØKELSE
Geological Survey of Norway

MAP 02
VLF, ORTHOGONAL

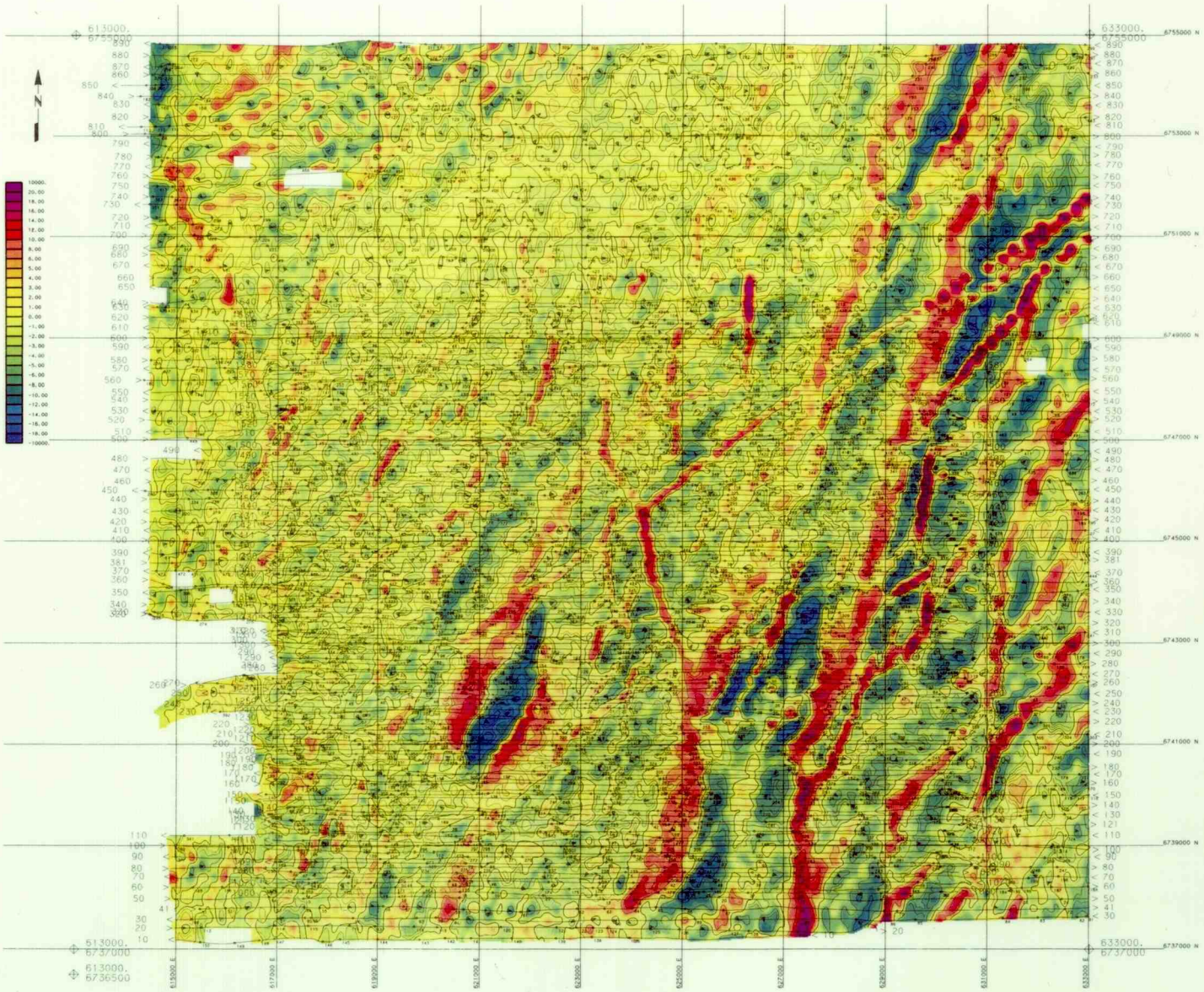

NGU
NORGES GEOLOGISKE UNDERSØKELSE
Geological Survey of Norway

MAP 03
VLF, INLINE

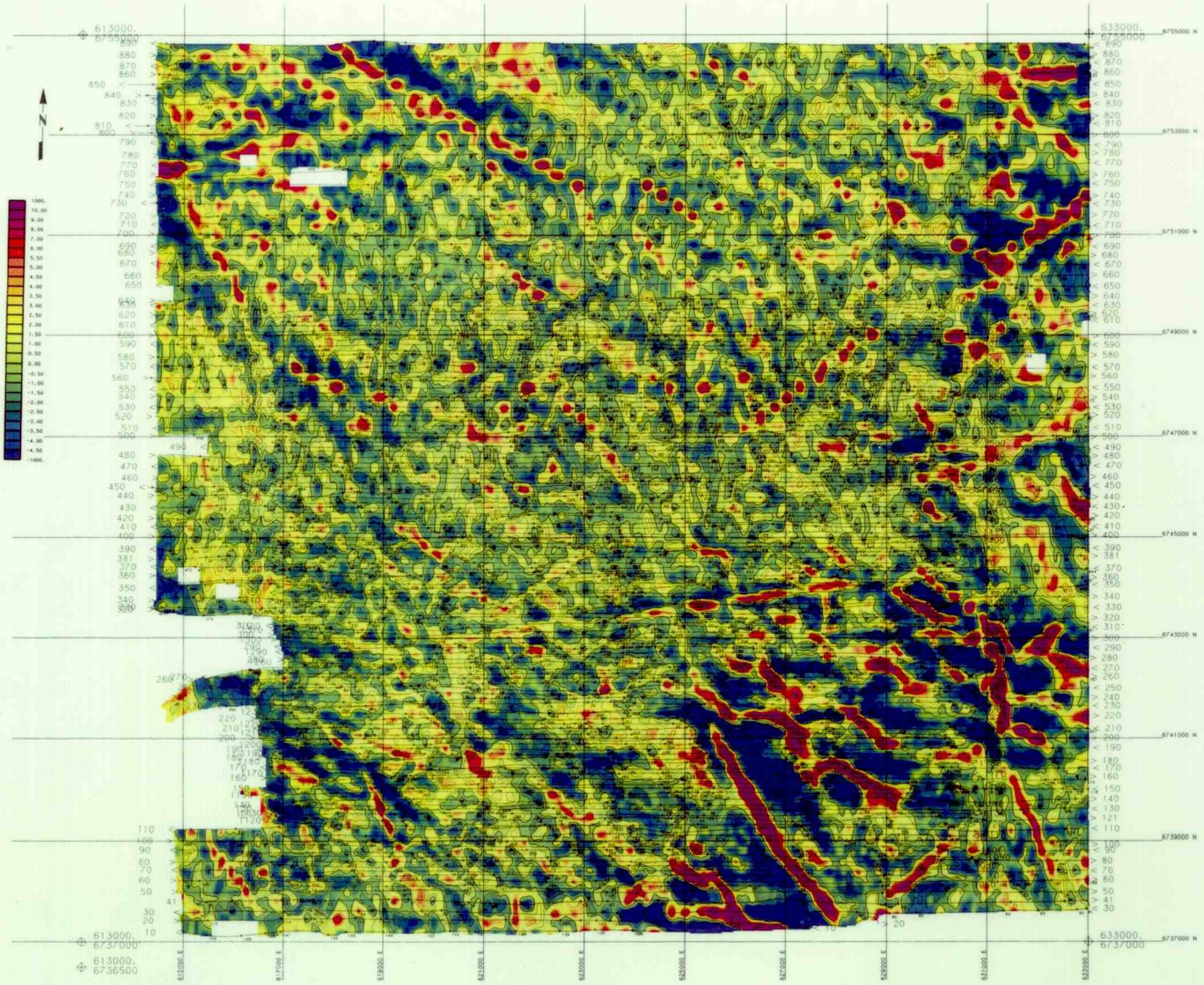

NGU
NORGES GEOLOGISKE UNDERSØKELSE
Geological Survey of Norway

MAP 04

4218 HZ APPARENT RESISTIVITY

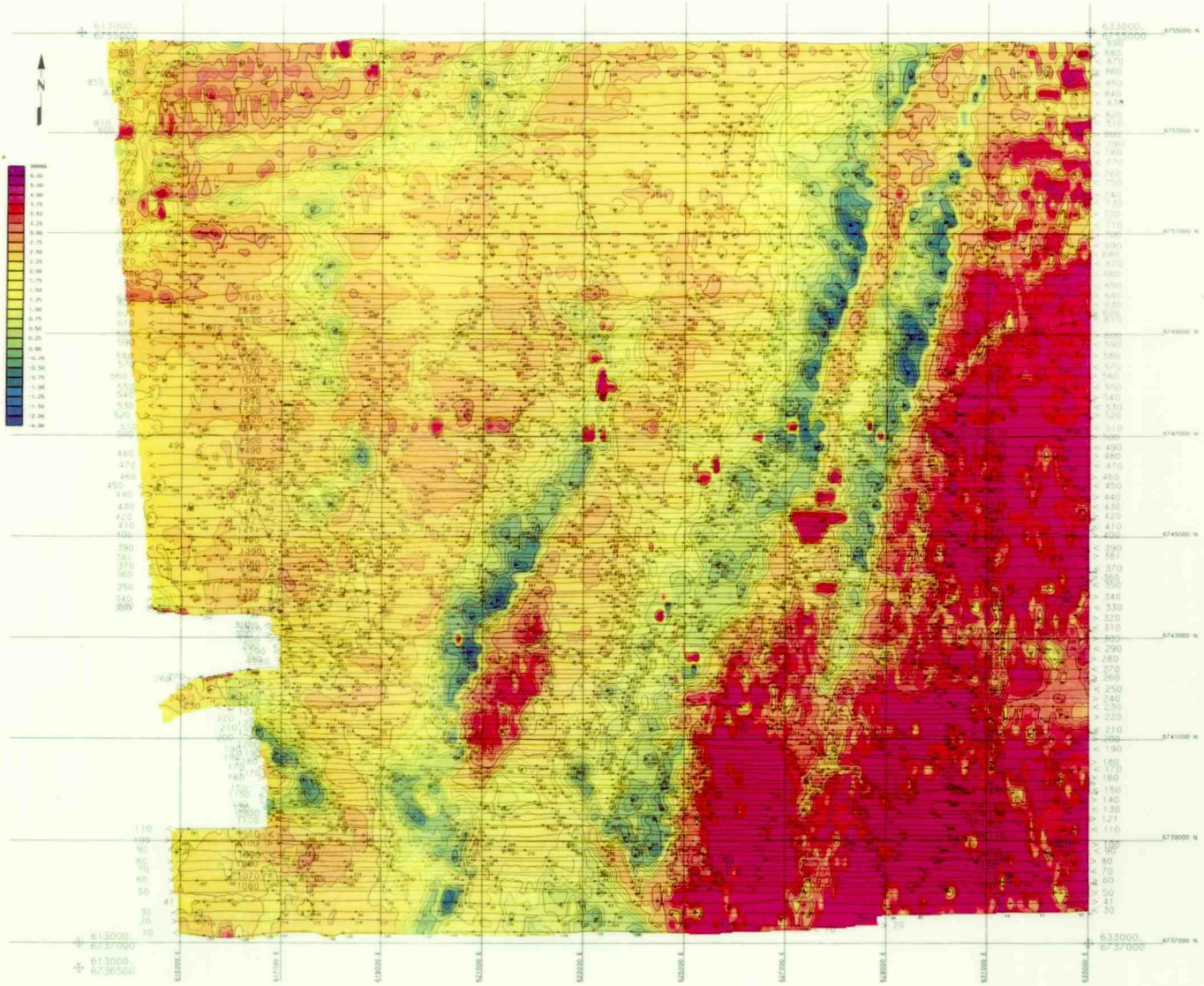

NORGES GEOLOGISKE UNDERSØKELSE
Geological Survey of Norway

MAP 05

34262 HZ APPARENT RESISTIVITY

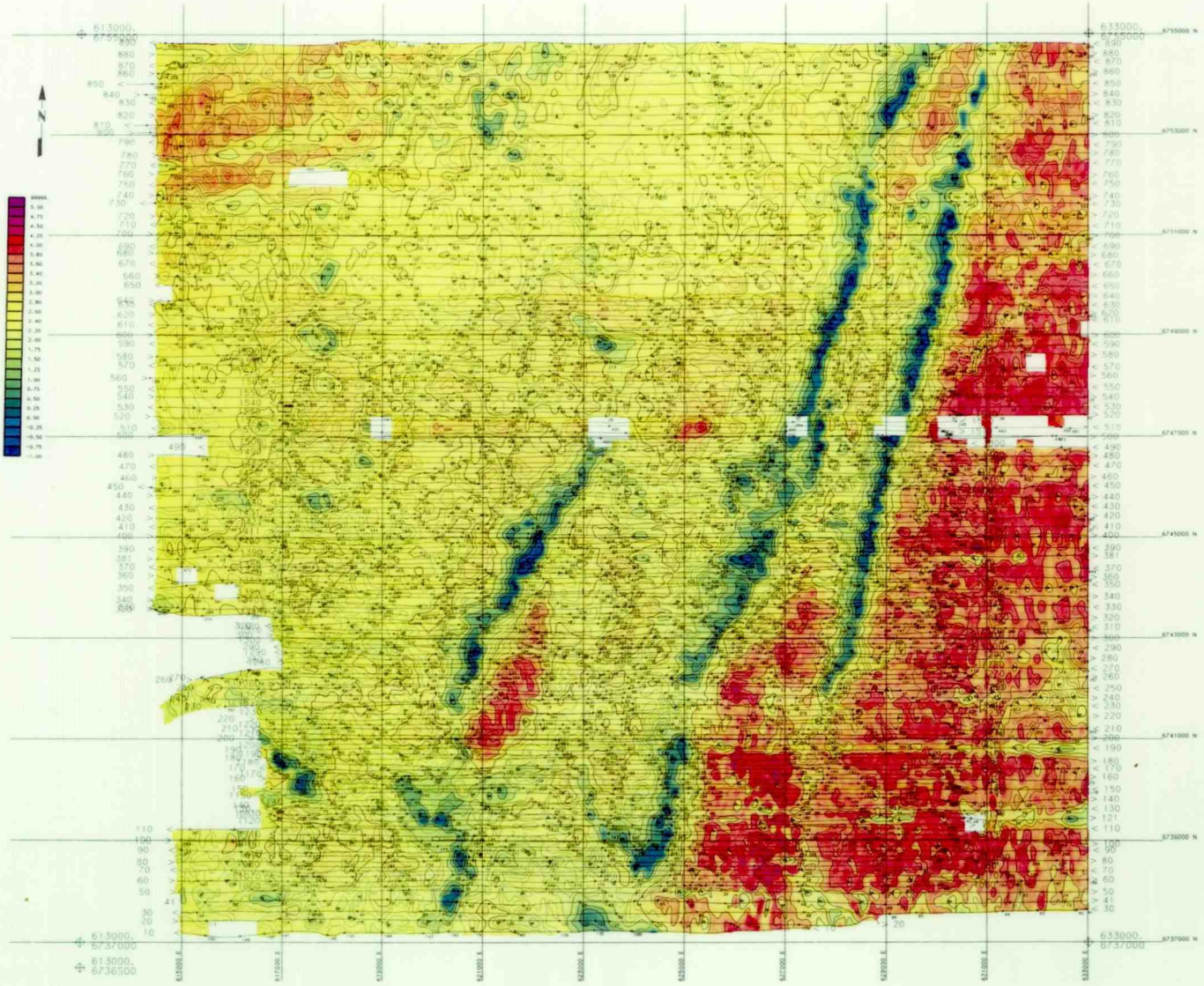

NGU
NORGES GEOLOGISKE UNDERSØKELSE
Geological Survey of Norway

MAP 06

4616 HZ APPARENT RESISTIVITY

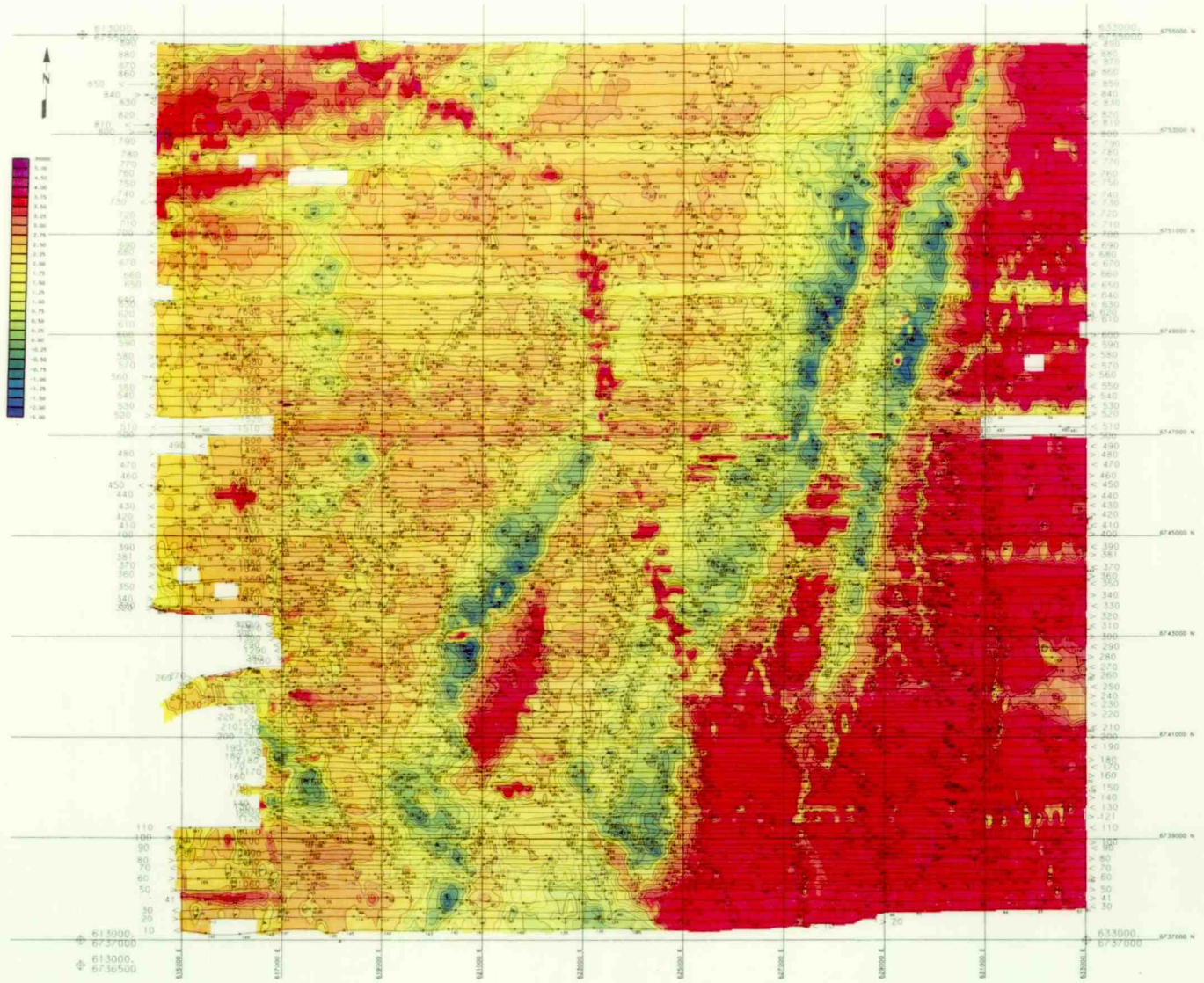

NGU
NORGES GEOLOGISKE UNDERSØKELSE
Geological Survey of Norway

MAP 07
POTASSIUM COUNTS

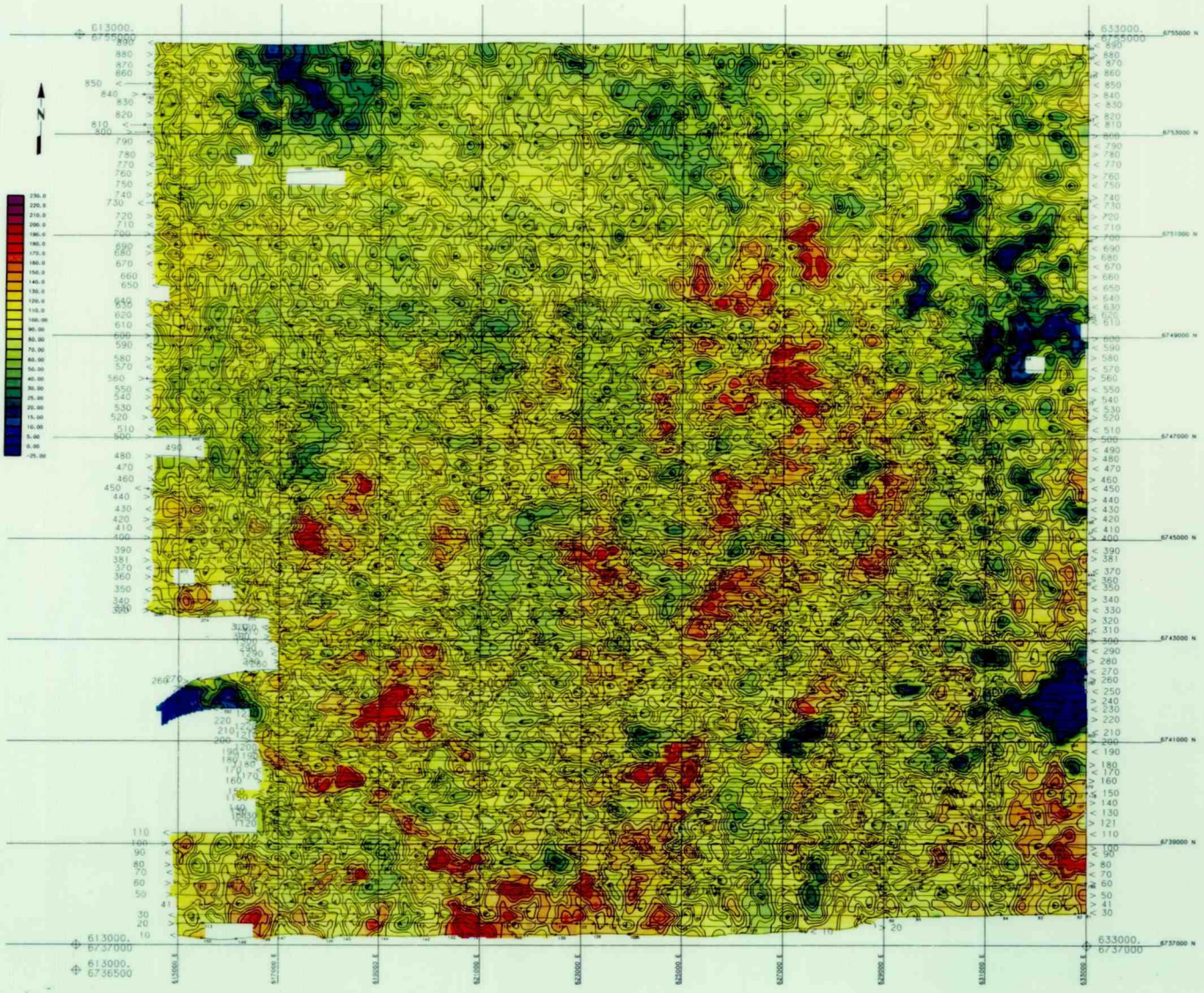

NGU
NORGES GEOLOGISKE UNDERSØKELSE
Geological Survey of Norway

MAP 08
URANIUM COUNTS

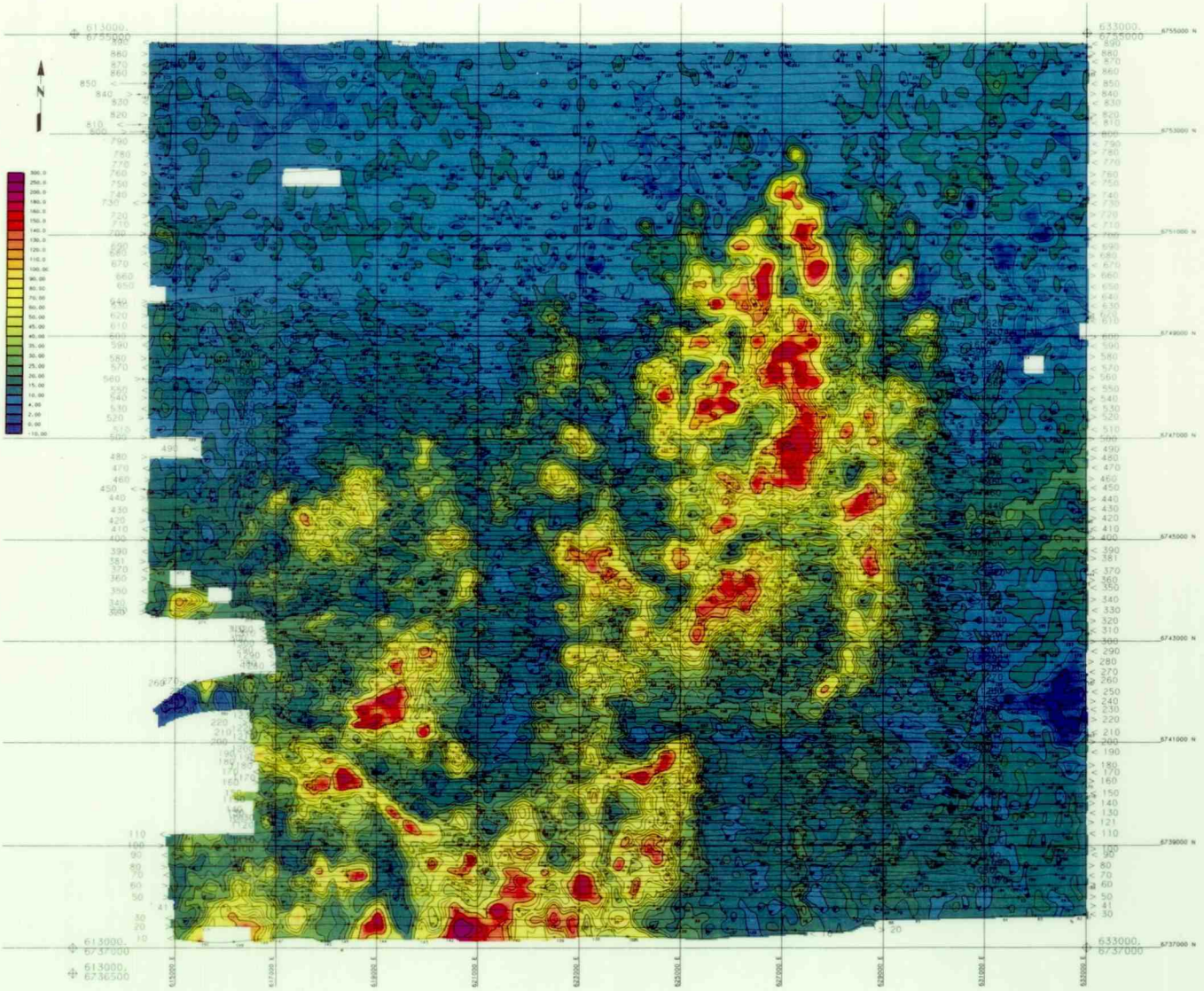

NGU
NORGES GEOLOGISKE UNDERSØKELSE
Geological Survey of Norway

MAP 09
THORIUM COUNTS

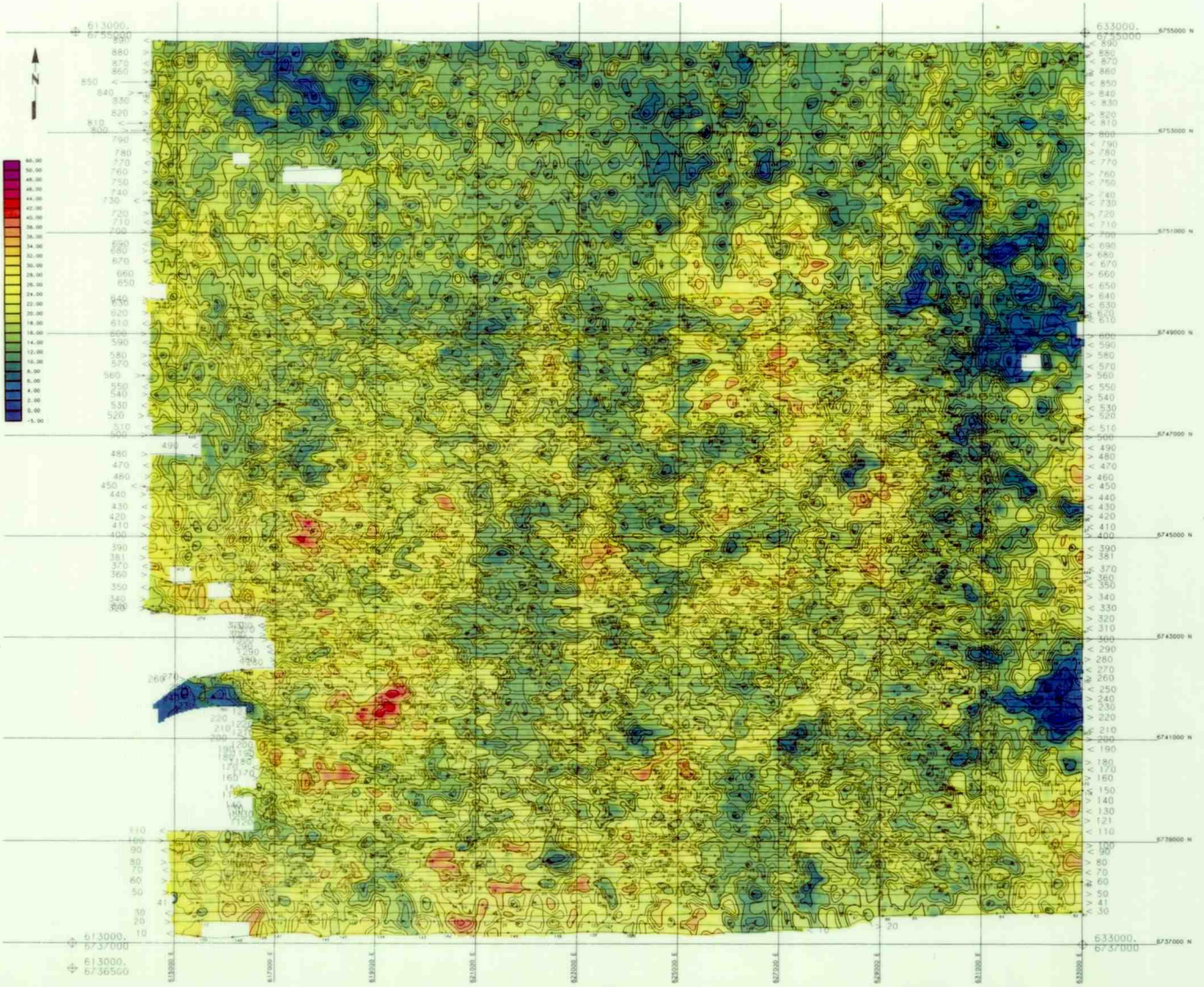

NGU
NORGES GEOLOGISKE UNDERSØKELSE
Geological Survey of Norway

MAP 10
POTASSIUM - URANIUM RATIO

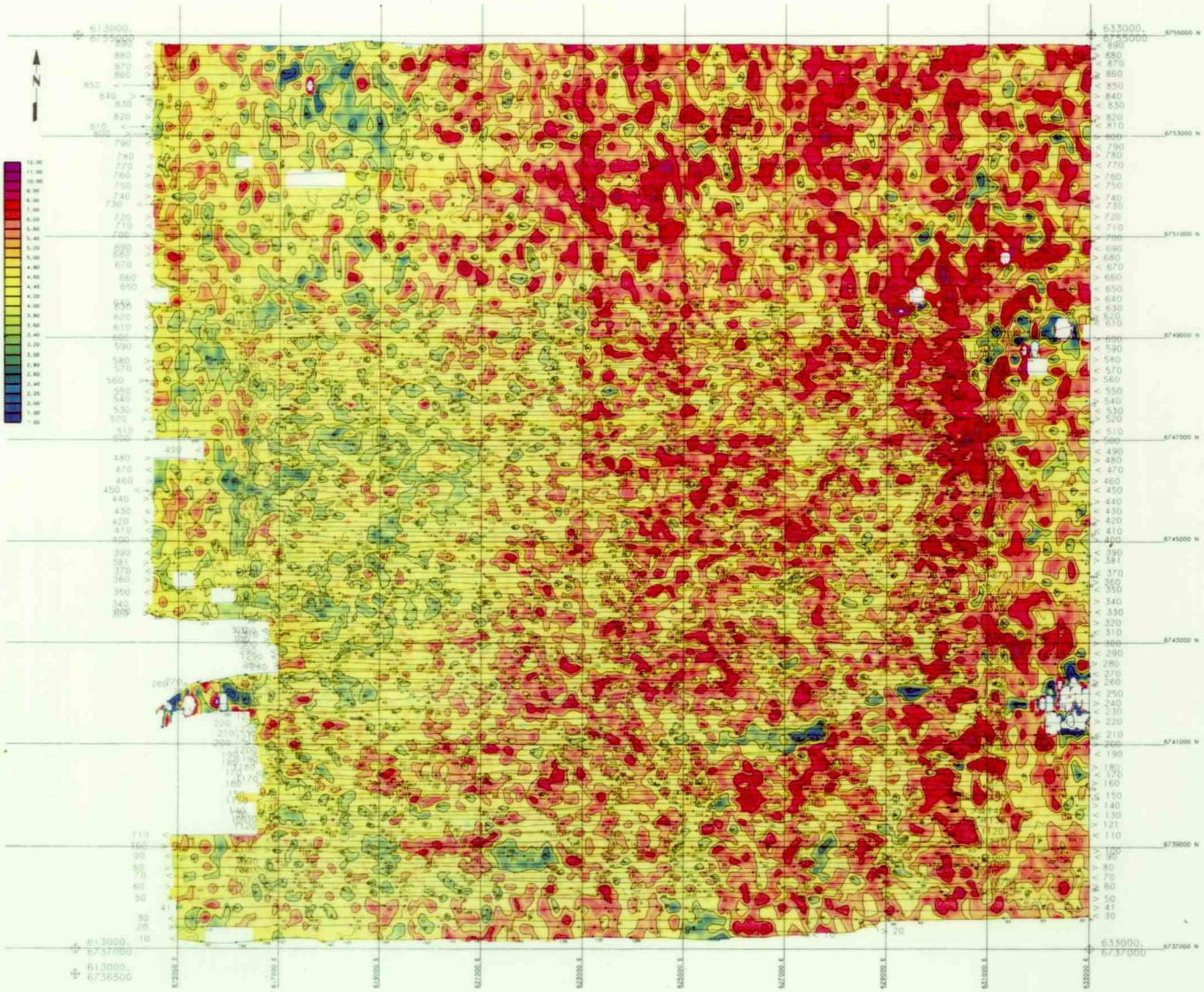

NGU
NORGES GEOLOGISKE UNDERSØKELSE
Geological Survey of Norway

MAP 11
POTASSIUM-THORIUM RATIO

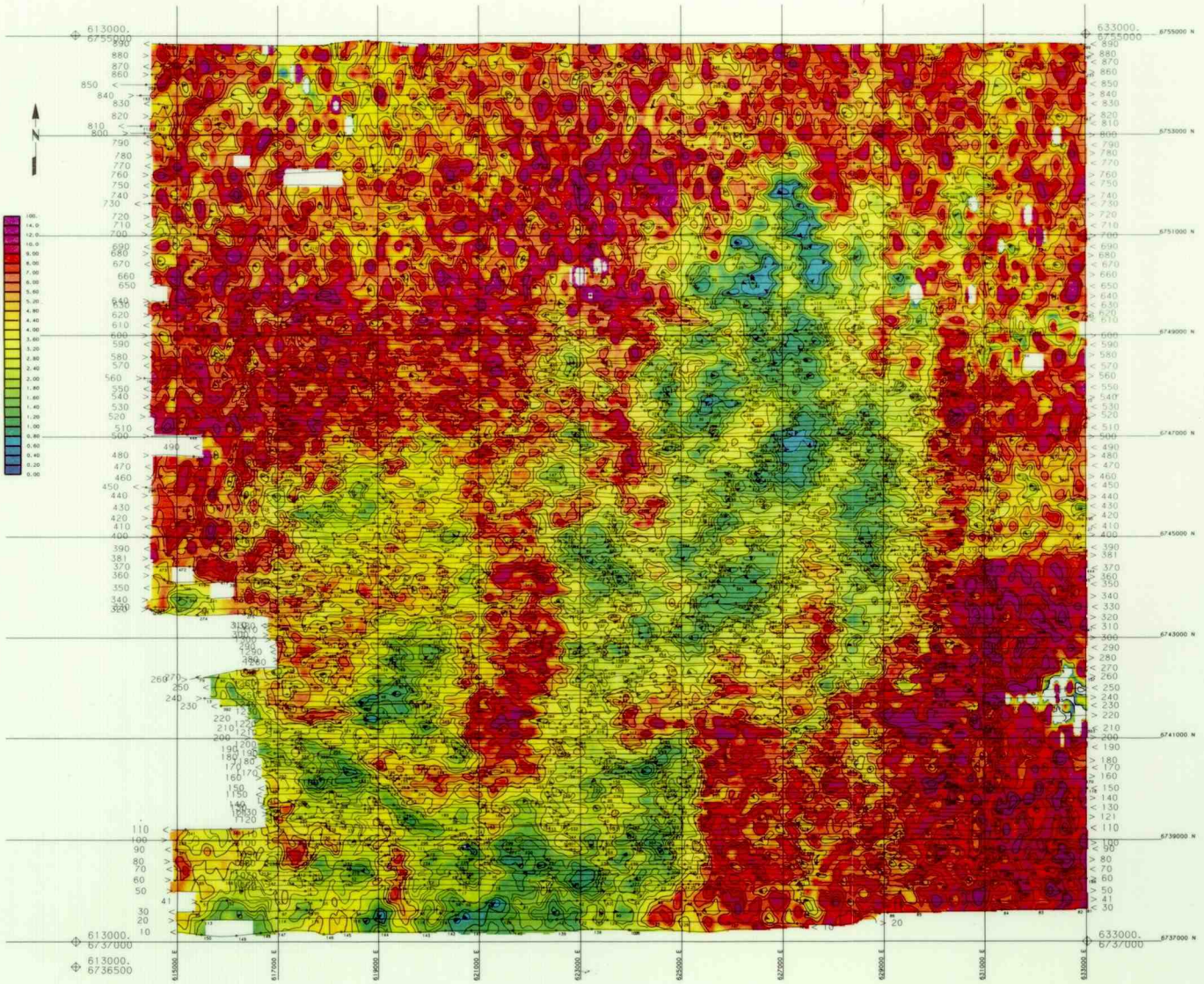

NGU
NORGES GEOLOGISKE UNDERSØKELSE
Geological Survey of Norway

MAP 12
URANIUM-THORIUM RATIO